

AUGMENTED VARIATIONAL SERIES AND HISTOGRAM-BASED CLUSTERING FOR UNIVERSAL IMPULSE DENOISING

KENNY KAL VIN TOH AND NOR ASHIDI MAT ISA

Imaging and Intelligent Systems Research Team
School of Electrical and Electronic Engineering
Engineering Campus, Universiti Sains Malaysia
14300, Nibong Tebal, Penang, Malaysia
kenny_tkv@ieee.org; ashidi@eng.usm.my

Received May 2011; revised October 2011

ABSTRACT. *This paper proposes a novel clustering approach for detecting impulse noise in digital images. From the clusters formed, we can identify the impulsive pixels in the noisy image. Combining it with a detail preserving noise filter using the switching framework, we obtain a high-performance two-stage algorithm for universal impulse denoising. As opposed to many existing filters that focus only on a particular impulse noise model, the proposed method, called the Augmented Variational Series and Histogram-Based Clustering (AVSHC) filter, demonstrates excellent performance in suppressing random-valued and fixed-valued impulse noise models, as well as a combination of both models. Extensive simulations conducted on monochrome test images under a wide range of impulse noise densities show that the AVSHC filter substantially outperforms other state-of-the-art impulse noise filters in terms of impulse detection, image restoration, and computational cost.*

Keywords: Impulse noise, Augmented variational series, Histogram processing, Clustering, Switching filters, Nonlinear filtering, Image restoration

1. Introduction. Visual data from digital images contain information that is critical for applications in a broad spectrum of research areas. Unfortunately, digital images are inevitably subjected to the contamination of impulse noise. Some likely causes of impulse noise include malfunctioning pixel sensors, faulty memory units, external disturbances in a noisy environment, imperfections encountered during transmission, electromagnetic disturbances, and timing errors in analog-to-digital conversion [1-3]. As a result, impulse noise may severely degrade the image quality and cause data pertaining to important features in the image to be significantly damaged.

In many applications, noisy images are preprocessed and restored in the early pipeline of image processing before subsequent image-processing tasks are performed. Preprocessing is imperative, and even indispensable, because the accuracy of subsequent operations (e.g., image classification, enhancement, segmentation, and parameter estimation) is largely affected by the quality of the filtered image [1, 3]. Recently, more image sensors per unit area are packed onto chips, and image capturing devices have become increasingly sensitive toward the exposure to impulse noise. In this respect, manufacturers of image capturing devices rely primarily on image denoising algorithms to improve the quality of the acquired image [4]. To this end, a number of techniques have been proposed for the removal of impulse noise [1-42].

Over the years, nonlinear filtering techniques have been considered state-of-the-art methods because of their impressive performance. Of these techniques, the median filter [5], which exploits the rank-order information within a filtering window, appears to be a

popular choice for suppressing impulse noise. Employed in a similar fashion to window-based filtering algorithms, the median filter is applied in a raster-scan order, and it treats all pixels equally, regardless of whether the pixels are corrupted or noise-free. Hence, local information consisting of image details and edges comprising noise-free pixels is a subject to be filtered. Ignoring such local information often results in desirable image details being at best blurred and at worst missing when the image is filtered. Nonetheless, this drawback has been overcome with the inception of the switching filters framework [1-3, 6-22].

The class of switching filters has been proven to be more effective than its nonswitching counterparts in many aspects, from detail preservation to noise suppression. Therefore, switching filters have become a powerful tool for impulse denoising. The crucial role of switching filters is to discriminate noise pixels from noise-free pixels prior to applying nonlinear filtering. The process of discriminating noise pixels from noise-free pixels can be accomplished by incorporating an impulse detector into the conventional filtering framework. However, early-developed switching filters [7, 9] are found to be nonadaptive toward impulse noise density variations [15]. At higher noise density interference, the impulse detectors are prone to yield pixel misclassifications. Thus, image details and edges are blurred, and undetected impulsive pixels create a strong negative visual effect on the filtered image.

In this paper, we classify existing switching filters into three categories: *nonadaptive* [1, 6-13], *adaptive* [3, 14-17], and *iterative* [18-22]. Within each category, more advanced techniques are integrated as part of the switching filters framework to obtain additional information about the image (e.g., local statistics and thresholds). It is observed that switching filters that use such additional information can enjoy performance improvements by their impulse detectors and/or filters. These sophisticated techniques include various types of filtering, including order-statistics [23-26], variational-regularization [3, 27, 28], soft computing [2, 29-37], mathematical morphology [38], threshold Boolean [39], and decision-based approaches [10, 40]. Technically, these high-complexity techniques are effective for switching filters because of their adaptive functionalities and advanced features to approximate nonstationary statistical characteristics of impulse noise [2].

Many of the methods mentioned above have the drawbacks of blurring finely textured image details, smearing thin lines, and distorting edges. Moreover, these methods are designed exclusively for filtering images that are heavily corrupted by a specific type of impulse noise model (e.g., see [16, 22]). By heavily corrupted, we mean the corruption of more than 25% of the total pixels. Less attention is given to the case of low corruption rates, in which precise impulse detection is highly desirable [23]. Although some methods can compensate for different impulse noise models with low noise density, loss of image details and over-smoothing of edges are still prevalent. Furthermore, methods that require training and tuning of parameters (e.g., see [2, 33]) are time consuming and less predictable when implemented [13]. These pitfalls, among others, mark the problems faced by the class of switching filters. Regardless of impulse noise density, good restoration can be attained but at the expense of increased computational cost. Roughly speaking, the great challenge in impulse denoising is to find the best tradeoff between impulse suppression and detail preservation. Moreover, the computational complexity needs to be kept low for reason to be cost effective in practical applications. Such observations motivated us to develop a fast and effective method for impulse denoising.

In this paper, we channel our attention toward developing a robust filter that can handle any type of impulse noise models and, therefore, can be considered a “universal” impulse noise filter. Our goal is to effectively suppress impulse noise while retaining finer details in the image. Therefore, we propose a novel two-stage method, called the

Augmented Variational Series and Histogram-Based Clustering (AVSHC) filter, based on the switching-scheme concept. The contributions of this paper are the following:

- We describe and propose two impulse detectors, one based on signal augmentation clustering and another based on histogram clustering, which can be easily combined to construct a universal impulse detector.
- We propose an adaptive median filter founded on fuzzy reasoning for accurate restoration.
- We develop a fast and automated stopping criterion for iterative switching filters that is based on a newly introduced image “roughness” index.

The advantages of the proposed method include:

- It removes fixed- and random-valued impulse noise, and any mixture thereof.
- It removes visible impulsive pixels as cleanly as possible while maintaining the detail information and natural appearance of the filtered image.
- It operates at a wide range of impulse noise densities without needing any burdensome tuning or tedious training of parameters when applied recursively and iteratively.
- It has low computational complexity and fast runtime.

The above advantages appear to greatly simplify camera design criteria as modern consumer cameras seek compact designs for image preprocessing. Instead of embedding multiple filters for removing different types of impulse noise, a single universal filter that offers competitive filtering performance is more preferable¹. Because impulse noise can exist in various stages in the canonical image processing pipeline or outside of the image formation process, impulse noise filters play a crucial role in improving the overall appearance of the captured image [1, 36]. This is particularly true for filters with universal behavior, such as the one proposed, and thus such filters have become an imperative design module among diverse image capturing devices. In fact, image applications in recent consumer electronic products often include a signal preprocessor customized with an impulse noise filter [9, 34]. In this regard, the proposed AVSHC filter emerges as a natural choice over other established impulse noise filters because of its competitive advantages and effectiveness. As will be seen later in this paper, simulation results reveal that both objective and subjective evaluations favor the AVSHC filter over other state-of-the-art impulse noise filters.

The outline of this paper is as follows. Section 2 reviews various types of impulse noise models. The design and implementation of the proposed filter are formulated in Section 3. Simulation results, comparisons, and discussions are provided in Section 4. Finally, the conclusion is presented in Section 5.

2. Impulse Noise Models. For clarity, we first discuss the different types of impulse noise models. Considering an image of size $M \times N$ stored as 8-bit grayscale pixel resolution, pixel intensities lie in the dynamic range $[I_{\min}, I_{\max}]$, in which I_{\min} and I_{\max} represent the lowest and highest intensities, respectively. Regardless of its origin, impulse noise randomly misfires a certain percentage of pixels with intensity values that are significantly different from the uncorrupted neighborhood. Thus, an image contaminated with impulse

¹In the classical camera design, multiple denoising methods, such as median filtering and weighted averaging, are embedded in the camera for preprocessing the captured image. Usually, the final image is averaged from the outputs of each filter. This design is typically slow and sometimes blurs the final image.

noise of probability² ρ can be modeled as:

$$x(i, j) = \begin{cases} f(i, j): & \text{with probability } \rho \\ o(i, j): & \text{with probability } 1 - \rho \end{cases} \quad (1)$$

where $x(i, j)$ denotes the pixel at location (i, j) with intensity x , and $f(i, j)$ and $o(i, j)$ represent the noisy and noise-free images, respectively.

Fundamentally, two types of impulse noise models are widely used in image processing literature: the random-valued impulse noise (RIN) model and the fixed-valued impulse noise (FIN) model. The former is also known as uniform impulse (UNIF) noise, in which the noise pixels can take any intensity values within the image dynamic range, i.e., $f_{unif}(i, j) \in [I_{\min}, I_{\max}]$. Alternatively, the FIN model assumes a limited number of impulsive intensities that appear in certain percentages; for examples, see [15, 30]. In a related note, the simplest and most frequently used FIN model in contemporary literature is salt-and-pepper (SNP) noise. Under the assumption of the SNP noise model, impulsive pixels are assumed to take the minimal and maximal intensities, i.e., $f_{snp}(i, j) \in (I_{\min}, I_{\max})$.

In reality, we have *a priori* knowledge about neither the impulsive amplitudes nor the impulse noise densities. In fact, impulse noise results from the interference of noise signals with arbitrary amplitudes. Consequently, the impulsive amplitudes could fall either inside or outside of the image dynamic range. When the impulsive amplitude lies within the image dynamic range, the corresponding pixel appears as UNIF noise in the noisy image. However, if the impulsive amplitude falls outside of the image dynamic range, the corresponding pixel is saturated and flipped to the maximal or minimal intensity and emerges as SNP noise. Under these circumstances, it is more appropriate to consider a more general impulse noise model.

Apparently, real impulse noise is a mixture of the SNP and UNIF noise models. For this reason, Petrovic and Crnojevic [33] have proposed a simplified but realistic impulse noise model that contains both the SNP and UNIF noise models. The general impulse noise model, called mixed impulse (MIX) noise, is given here as:

$$x(i, j) = \begin{cases} f_{unif}(i, j) & : \text{ with probability } 0.5\rho \\ f_{snp}(i, j) & : \text{ with probability } 0.5\rho \\ o(i, j) & : \text{ with probability } 1 - \rho \end{cases} \quad (2)$$

In this way, half of the impulsive pixels are modeled as SNP noise, and the remaining half are modeled as UNIF noise. If we think of impulse noise in image degradation as a combination of two independent processes of injecting the image with $f_{snp}(i, j)$ and $f_{unif}(i, j)$, the question of choosing an appropriate impulse noise model is reduced to the selection of the MIX noise model. We advocate the use of the MIX noise model in (2) because it is deemed more suitable and reasonable when testing the performance of an impulse noise filter. Thus, we will pay particular attention to the MIX noise model, although the universality of the AVSHC filter can also produce impressive results when restoring images contaminated with SNP or UNIF noise models.

3. Formulation and Implementation. In this section, we present a detailed description of the development of the AVSHC filter. We adopt a two-stage switching-scheme concept in which the first-stage impulse detection is cascaded with the second-stage impulse cancellation. These two stages are iteratively executed until the stopping criteria for iteration, which is based on an image “roughness” index, is satisfied. Figure 1 shows the overall system architecture of the proposed AVSHC filter.

²Impulse noise probability and density both refer to the percentage of corrupted pixels; thus, these two terms are used interchangeably in the literature.

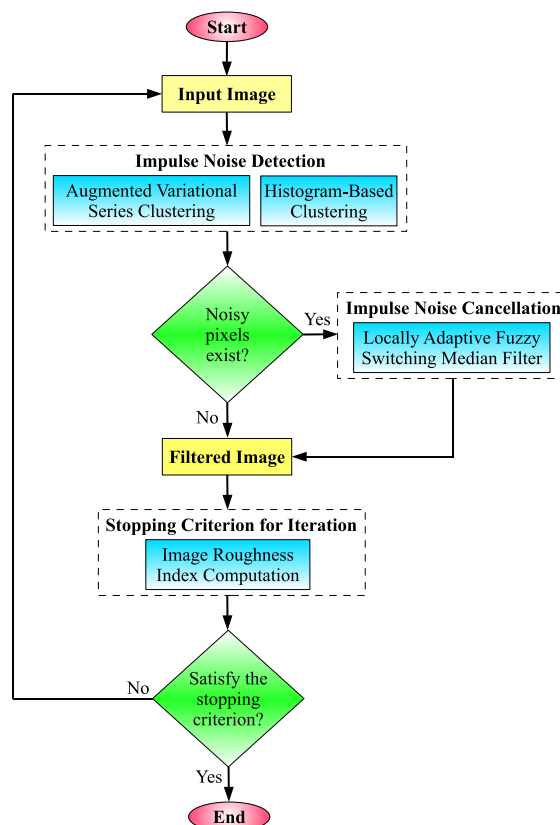


FIGURE 1. The system architecture of the AVSHC filter

For impulse detection, the impulse detectors attempt to distinguish noise pixels from noise-free pixels. In this case, our main aim is to handle separately pixels corrupted by the RIN distribution and those of the FIN distribution. This novel feature is critical because it combines flexibility and effectiveness in removing any kind of impulse noise. Initially, the first impulse detector segregates the pixels in a local window patch into several clusters according to their augmented variational series. Then, the second impulse detector further scrutinizes the isolation of impulsive pixels by segmenting the noisy image histogram into noise and noise-free clusters. By combining the outcomes of these two impulse detectors, we can easily distinguish the impulsive pixels because noise-free pixels may be grouped into a single cluster and the noisy pixels into other clusters. Subsequently, the detected noise pixels are subjected to the next stage for filtering, or filtering is bypassed if the pixels are classified as noise-free. As a result of this bypassing, the integrity of the underlying fine details and textures in the image can be preserved better. For impulse cancellation, we adopt an adaptive median filter to perform restoration on the noise pixels that are detected. In addition, fuzzy reasoning is exploited to assist in handling uncertainties present in the extracted local information.

In this framework, the proposed AVSHC algorithm is recursively implemented in an iterative manner. The filtered image in the current iteration is used as the input image for the subsequent iteration. An advantage of the iterative strategy is that some impulsive pixels located in the middle of large noise blotches can be gradually filtered after each iteration. Then, the recursive implementation can achieve better performance than the nonrecursive implementation because the newly restored pixel value takes effect immediately when the adjacent pixel is inspected by the impulse detectors. As a result, at least one-half of the pixels in the local window patch are composed of either noise-free pixels

or previously restored pixels when they are recursively implemented. Additionally, the recursive behavior of the AVSHC filter speeds its runtime by preventing it from performing any unnecessary processing of noise-free pixels. As opposed to other methods that only adopt either recursive (see [1, 7, 10]) or iterative (see [18, 20, 28]) implementation, we combine both implementations to exploit the advantages of each and overcome their intrinsic disadvantages.

3.1. Impulse noise detection: cluster-based impulse detectors. Because the intensity of an impulsive pixel is significantly different from the other pixels in its surroundings, a noise pixel can be easily identified by an impulse detector by the height of the brightness jump in comparison with its neighboring pixels. Therefore, impulse detection can be performed by analyzing the local image statistics within a window patch the size of which is bounded by the detector.

Let W_d denote the local window with odd $(2K_d + 1) \times (2K_d + 1)$ dimensions centered at $x(0, 0)$, i.e.,

$$W_d = \{(k, l) \mid -K_d \leq k, l \leq K_d\}, \quad (3)$$

and let the set of neighboring pixels $x(i + k, j + l)$ be

$$W_n = \{x(i + k, j + l) \mid (k, l) \in W_d, (k, l) \neq (0, 0)\}. \quad (4)$$

If the pixels in W_n are sorted in ascending order as

$$W_s(1) \leq W_s(2) \leq W_s(3) \leq \dots \leq W_s((2K_d + 1)^2 - 1), \quad (5)$$

we can denote the sorted neighborgram as W_s , given by:

$$W_s = \{W_s(1), W_s(2), W_s(3), \dots, W_s((2K_d + 1)^2 - 1)\}. \quad (6)$$

Subsequently, the variational series V is obtained by computing the absolute differences between the adjacent pixel intensities in the sorted neighborgram, i.e.,

$$V(m) = |W_s(m + 1) - W_s(m)| : m = 1, 2, \dots, (2K_d - 1)^2 - 2. \quad (7)$$

As mentioned earlier, impulsive pixels often exhibit intensities that vary greatly from those of their neighbors. In this case, large absolute differences are produced in the variational series, and impulsive pixels can be easily identified by the impulse detector. However, one difficulty arises when some impulsive intensities are near those of their neighboring pixels, in which case the absolute differences may not be large enough for the impulse detector to distinguish impulsive pixels from noise-free pixels. Consequently, one of the following two errors may occur: impulsive pixels can be misinterpreted as finely textured image details and, thus, remain unaltered, or finely textured image details can be mistaken for impulsive pixels and, therefore, filtered from the image. The first type of error may adversely affect the filtered image quality even if only a few impulses are retained whereas the second type of error may unnecessarily cause image details to be removed.

One way to minimize the possibility of these errors occurring is to amplify the absolute intensity differences in $V(m)$ and yet keep the small differences from increasing too much. In this case, we use a piecewise-linear fuzzy set $\mu(m)$ with adjustable parameters to accomplish this goal. Given the intrinsic vagueness within the noise and noise-free pixels that gives rise to the two types of errors, the line of fuzzy reasoning is an effective tool for handling the vagueness and uncertainty present in the image data [6]. Applying $\mu(m)$

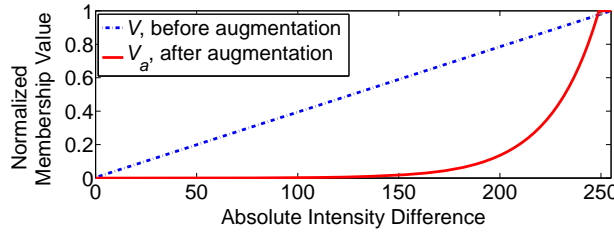


FIGURE 2. The plot of the variational series V and augmented variational series V_a versus the absolute intensity difference. Note that the impulse detection mechanism of some well-known methods [7-9, 15-22, 26-34] is represented by V (i.e., before signal augmentation) whereas our impulse detection based on signal augmentation approach is represented by V_a .

on $V(m)$, we get

$$\mu(m) = \begin{cases} 0.0 & : V(m) \leq F_1^{(t)} \\ \frac{V(m)-F_1^{(t)}}{F_2^{(t)}-F_1^{(t)}} & : F_1^{(t)} < V(m) < F_2^{(t)} \\ 1.0 & : V(m) \geq F_2^{(t)} \end{cases} \quad (8)$$

where $F_1^{(t)}$ and $F_2^{(t)}$ are two adaptive thresholds in the t th iteration ($t \geq 1$). Within the dynamic range $\mu(m) \in [0, 1]$, $\mu(m)$ is kept low if the absolute differences in variational series $V(m) \leq F_1^{(t)}$ and the absolute differences in $V(m)$ are fully amplified when $V(m)$ surpasses the limit defined by $F_2^{(t)}$. Then, the variational series can be augmented using

$$V_a(m) = \exp [10 \cdot \mu(m)] - 1.0 \quad (9)$$

where $V_a(m)$ represents the augmented variational series.

By considering all possible absolute differences between two pixel intensities (i.e., $V(m) \in [I_{\min}, I_{\max}]$), we show the effect of signal augmentation by comparing the membership values (normalized to the dynamic range $[0, 1]$) for $V(m)$ and $V_a(m)$ in Figure 2. Generally, we plot the normalized functions for (7) and (9) in Figure 2 with $F_1^{(1)} = 10$ and $F_2^{(1)} = 250$. Although $V(m)$ represents the absolute difference between two adjacent intensities in the sorted neighborgram W_s , it can also serve as the absolute intensity difference between a center pixel and one of its neighboring pixels as in conventional switching median filtering. In other words, $V(m)$ in (7) represents the core detection mechanism of various well-known switching median filters, such as those in [7-9, 15-22, 26-34]. Accordingly, we note that the proposed signal augmentation is an additional step to improve the accuracy of the impulse detection mechanism employed by these filters. From Figure 2, the normalized membership value curve for $V_a(m)$ is upward sloping, and it increases faster as the absolute intensity difference increases. In contrast, the normalized membership value curve for $V(m)$ increases linearly with the absolute intensity difference. This linear characteristic contributes to the errors perpetuated by conventional switching median filters by mistakenly treating high-contrast local image contents (such as edges and thin lines) as impulse noise, and vice versa.

We argue that such errors can be reduced by using signal augmentation because small irregularities in absolute intensity differences are neutralized whereas medium and large absolute intensity differences are further intensified. To support this claim, we perform an experiment by analyzing the performance of the impulse detector before and after signal augmentation. Specifically, we test the accuracy of the impulse detection using $V(m)$ and $V_a(m)$ in (7) and (9), respectively. Again, we clarify that the impulse detection

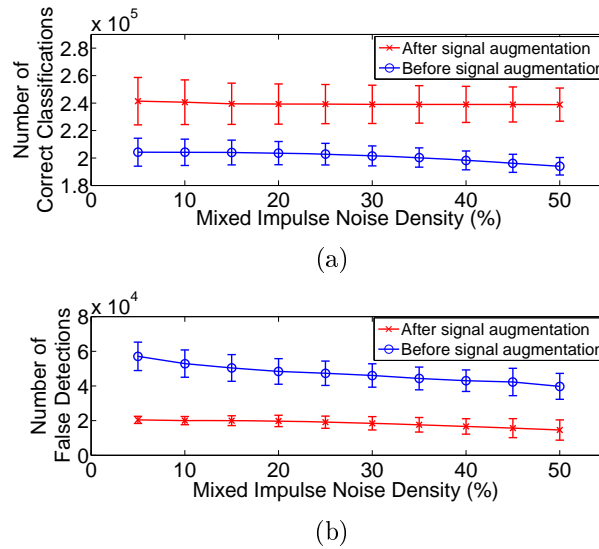


FIGURE 3. Comparison of the effectiveness in impulse detection performance before and after signal augmentation

based on $V(m)$ represents the impulse detection mechanism of some previously mentioned switching median filters whereas the mechanism based on $V_a(m)$ represents our proposed impulse detection. In this experiment, we artificially inflict 5% to 50% of MIX noise (as modeled in (2)) in 5% noise steps on a set of 10 standard test images³ before running the impulse detector twice on each image; the impulse detector is tested initially without signal augmentation and later with signal augmentation. The conditions for classifying noise and noise-free pixels are similar to those in [7]. For simplicity, we execute the impulse detector once (i.e., $t = 1$), and we select $K_d = 1$, $F_1^{(1)} = 10$, and $F_2^{(1)} = 250$. We assume that the locations of all the noise and noise-free pixels are known in advance, and then the impulse detector attempts to classify all of the pixels into two groups: the noise pixels set and the noise-free pixels set.

The outcome of the experiment is shown in Figure 3 as the error bar charts for comparing the statistics on impulse detection performance (i.e., the average number of correct classifications and false detections⁴) before and after signal augmentation. The error bars represent the standard deviations of impulse detection statistics and the heights of the bars reveals how tightly the accuracy of the impulse detection statistics is clustered around the means. We can see from Figure 3(a) that the error bars for correct classification have greater height after signal augmentation. This result concurs with our earlier argument that the signal augmentation process increases the accuracy of the impulse detector. Furthermore, the height of the bars remain constant across a wide density of impulse noise, which suggests that signal augmentation works well even when the image is highly corrupted with impulse noise. In the second plot in Figure 3(b), the impulse detector employing signal augmentation has shorter error bars than the one without signal augmentation. The smaller height demonstrates that the signal augmentation process minimizes the risk of false detections. In summary, signal augmentation introduces good

³The set of 10 standard test images used throughout this paper are the grayscale “Airplane,” “Baboon,” “Boat,” “Bridge,” “Cameraman,” “Goldhill,” “Lake,” “Lena,” “Pepper,” and “Pentagon” images of size 512×512 .

⁴The number of correct classifications is defined as the sum of correctly identified impulses and noise-free pixels by the impulse detector. The number of false detections is interpreted as the number of incorrectly identified noise-free pixels.

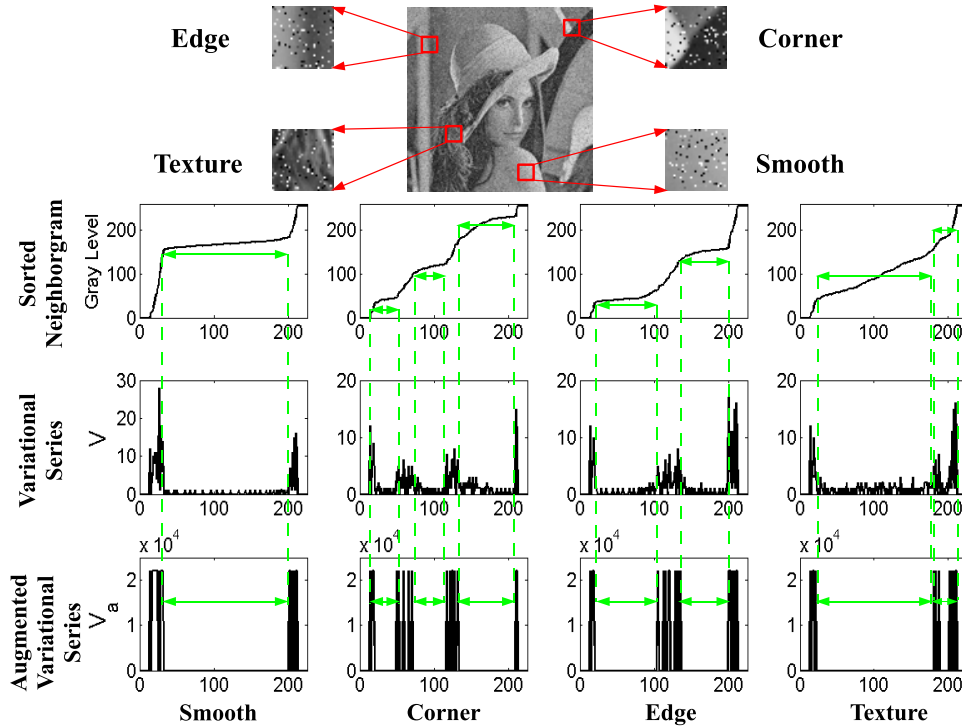


FIGURE 4. Illustration on the signal augmentation process using a 15×15 neighborhood for a variety of image local features: corner, edge, smooth, and texture. Note that the areas bounded by the arrows represent the range of the noise-free intensities.

noise tolerance into the impulse detector and increases the detection accuracy while reducing the risk for false detections. These criteria are highly desirable for a good impulse detector framework.

Figure 4 translates the theoretical concept of signal augmentation into action. In addition, we show evidence that the augmented variational series $V_a(m)$ is more useful than the widely used variational series $V(m)$, which does not apply signal augmentation. Clearly, $V_a(m)$ has the advantage of easily distinguishing impulsive pixels from noise-free pixels, even with the presence of delicate details in different image structures. For convenience in illustration, we perform signal augmentation on a 15×15 neighborhood (i.e., $K_d = 7$) for various image structures, such as corner, edge, smooth region, and texture. We note that small irregularities, which are composed of pixels with similar local features, that exist in the variational series $V(m)$ are smoothed upon augmentation whereas medium and large bumps in $V(m)$, because of the presence of impulse noise, are uniformly amplified. Likewise, it can be observed that $V_a(m)$ has discontinuities in its augmented variational series under the presence of impulse noise. These discontinuities support our intuition to classify noise-free pixels into a noise-free cluster and noise pixels into other clusters. However, it is trivial to observe that the discontinuities serve as boundaries that separate noise-free pixels from noise pixels. The nontrivial part of the process is to locate every cutoff point in the augmented variational series $V_a(m)$ with minimal mathematical requirements. To conduct the search for discontinuities in the augmented variational series, we employ a predefined threshold T_c on $V_a(m)$. From T_c , we are able to determine the occurrence of discontinuities in $V_a(m)$. Consequently, the number of clusters n , into which all W_s can be classified, is determined using

$$z \leftarrow z + 1 \Leftrightarrow V_a(m) > T_c \tag{10}$$

where $z = 1$ initially. Accordingly, the pixels in the set of sorted neighborgrams W_s are segmented into the z th cluster

$$C(z) = \{W_s(n) | n = 1, 2, 3, \dots, (2K_d + 1)^2 - 1\}. \quad (11)$$

All of the sorted neighboring pixels W_s are featured in the cluster $C(z)$ as long as the criterion $V_a(m) \leq T_c$ is satisfied. Initially, $C(1)$ contains its fixed member $W_s(1)$. Then, the condition in (10) is evaluated. If $V_a(m) > T_c$, $W_s(n + 1)$ falls into a new cluster, $C(z + 1)$, i.e., $C(2) = \{W_s(2)\}$. Otherwise, $W_s(n + 1)$ remains in the $C(z)$ cluster, i.e., $C(1) = \{W_s(1), W_s(2)\}$. The whole clustering process is repeated until m and n reach their maximum count of $(2K_d + 1)^2 - 2$ and $(2K_d + 1)^2 - 1$, respectively. The largest cluster C_L that contains the most members represents the set of noise-free pixels in the local window W_d . For the case in which there is more than one cluster with equal size contending for C_L , cluster $C(z)$ with the smallest standard deviation is chosen because the smaller standard deviation corresponds to pixels having smaller absolute intensity differences [33]. Theoretically, a maximum of $(2K_d + 1)^2 - 1$ clusters may be formed when applying (10); however, this situation almost never occurs, which is not surprising because the above claim can be justified from the strategy adopted by the AVSHC filter. The recursive implementation ensures that W_d contains at least half of the neighbors with similar intensities, even for pixels on the edges [3]. However, the iterative implementation gradually decreases the number of corrupted pixels in W_d . These implementations reduce the total number of clusters and increase the membership in the noise-free cluster. Correspondingly, the same arguments apply to the case in which the number of noise-free pixels in a cluster equals that of the noise pixels in another cluster. It is worth mentioning that C_L can be found in a straightforward manner, and the tendency for a tie to form among clusters with maximum memberships almost never occurs.

The impulse detection accuracy can be improved by widening the boundaries of C_L . If we denote the lowest and highest intensities in C_L as I_{lower} and I_{upper} , respectively, we find through experimentation that some noise-free pixel intensities may lie slightly outside of the dynamic range $[I_{lower}, I_{upper}]$ but within a standard deviation away from I_{lower} and I_{upper} . To avoid misclassifying such pixels as noisy, we widen the boundaries between I_{lower} and I_{upper} by subtracting and adding the standard deviation σ_{C_L} of C_L , from I_{lower} and to I_{upper} , respectively. In practice, the standard deviation is more robust than the average absolute intensity differences when the number of sample data is small. Furthermore, we can adaptively extend the range of C_L by using its standard deviation to conform with the ‘‘spreadness’’ of the pixels data without risking the inclusion of impulsive pixels. If we define LB and HB as the respective new lower and upper boundaries, LB and HB can be calculated using:

$$LB = I_{lower} - \sigma_{C_L}, \quad (12)$$

$$HB = I_{upper} + \sigma_{C_L}. \quad (13)$$

The center pixel $x(i, j)$ is identified as a noise pixel if its intensity lies outside of the new dynamic range $[LB, HB]$. Otherwise, $x(i, j)$ is considered a noise-free pixel. An example of the impulse detection using augmented variational series clustering is shown in Figure 5, with $K_d = 1$, $F_1^{(1)} = 10$, $F_2^{(1)} = 250$, and $T_c = 5$. This part of the proposed impulse detection algorithm is sufficient to handle impulse noise density as high as 35%, but mainly for the RIN model. Nevertheless, we can operate the proposed impulse detection algorithm at a wider range of impulse density variations by easily incorporating an extra step for accurate detection of the FIN model.

Taking the FIN into account, we will use the global statistics of the noisy image histogram in detecting the fixed-valued impulsive intensities. The FIN model, which has a

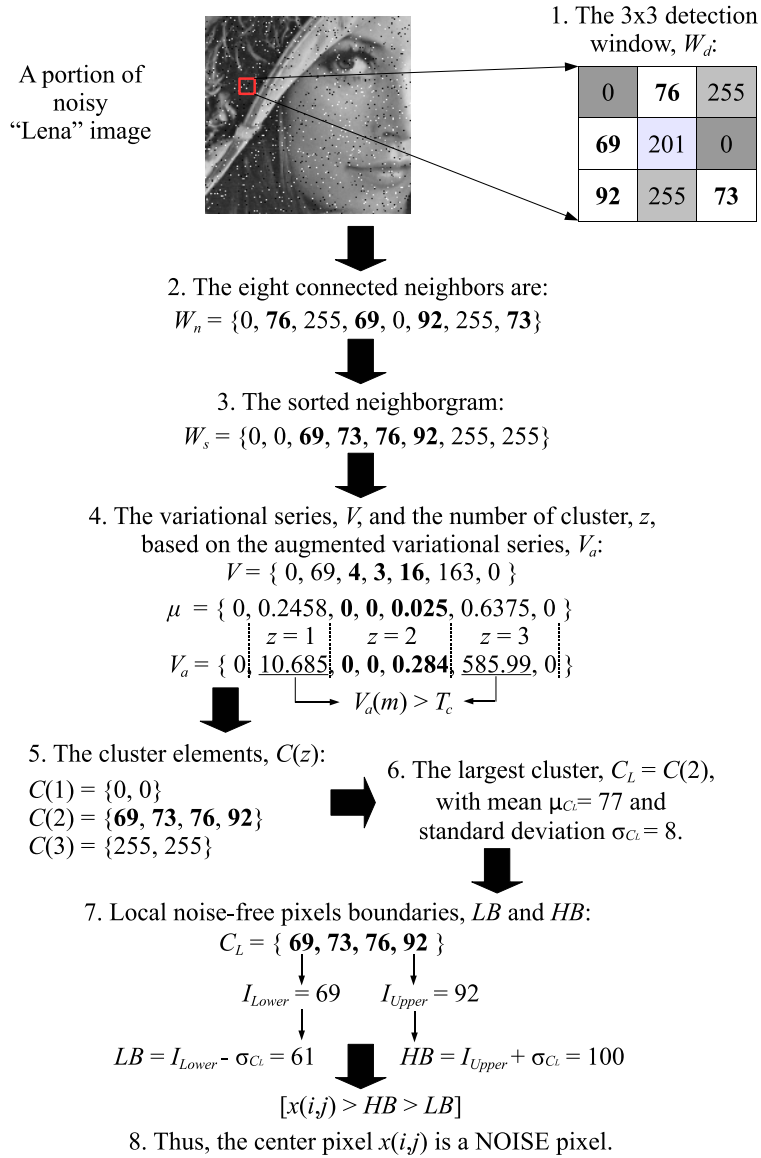


FIGURE 5. An illustration of the augmented variational series clustering algorithm. Note that noise-free pixel intensities and their corresponding computed elements are displayed in bold.

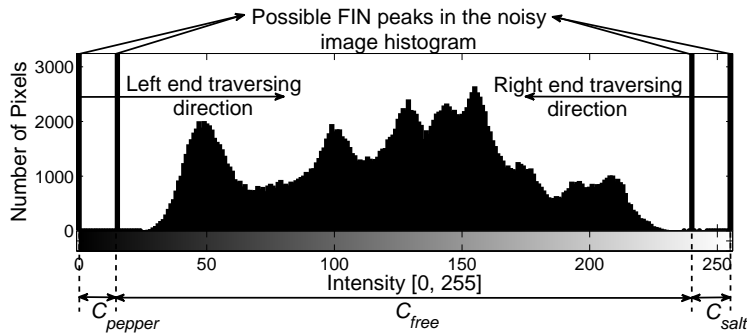


FIGURE 6. Histogram of “Lena” image corrupted with a general model of FIN. Impulsive peaks can be gradually removed after a few iterations using histogram-based clustering.

long-tailed noise distribution, can be easily detected by analyzing the noisy image histogram. Isolated peaks with extremal values in the noisy image histogram will point to the amplitudes of impulsive pixels [33]. Furthermore, it has been shown that peak intensities located at the ends of the noisy image histogram represent the fixed-valued impulsive intensities [1, 17, 33].

Basically, the FIN impulsive intensities can be found by simultaneously traversing the noisy image histogram from both ends toward the center of the histogram. We suggest the use of a local maximum in detecting the peak intensities. The local maximum in this context represents the first peak encountered when traversing the noisy image histogram in a particular direction (see Figure 6) [1, 17]. Therefore, our search for the peak intensities is immediately halted once the local maximums from both ends in the noisy image histogram are found. If the two local maximums encountered are denoted as I_{salt} and I_{pepper} , we may segment the noisy image histogram into three clusters, namely, a noise-free cluster $C_{free} \in [I_{pepper} + 1, I_{salt} - 1]$, a pepper-noise cluster $C_{pepper} \in [I_{min}, I_{pepper}]$, and a salt-noise cluster $C_{salt} \in [I_{salt}, I_{max}]$. If the intensity of the center pixel $x(i, j)$ falls within the C_{free} cluster, it is considered noise-free; otherwise, $x(i, j)$ is classified as a noise pixel.

The rationale in designing an impulse detector incorporating two different mechanisms for accurate impulse detection is deeper than merely imposing a single mechanism that handles both FIN and RIN noise models. Occasionally, FIN and RIN models demonstrate contradicting characteristics, and the fact that edges and thin lines in an image can be heavily disguised as impulse noise further complicates the noise detection process. Furthermore, the FIN model is frequently constructed as SNP noise on the basis of the assumption that noise pixels assumed only the two extreme values in the image dynamic range. This assumption, which has been extensively studied in some previous studies of SNP denoising [6-10, 15-17, 24, 26], does not hold true in real-world applications. Under some unavoidable circumstances, the SNP noise pixels may be replaced by close approximations of their actual fixed-valued impulsive intensities. For example, the extremal SNP noise intensities $I_{pepper} = 0$ can be substituted with gray levels 1 or 2, and $I_{salt} = 255$ with gray levels 254 or 253, for an image stored as an 8-bit integer. We illustrate this viewpoint in Figure 6 with the fixed-valued impulsive peaks at both ends of the histogram representing possible FIN peaks in real applications. In this case, impulse detectors (e.g., in [9] and [16]) that assume the fixed-valued impulsive intensities are composed of I_{min} and I_{max} suffer from truism and will fail to detect impulsive pixels present in the noisy image. However, our proposed impulse detector can perform well even with the presence of more than two FIN peaks. Impulsive FIN peaks situated near the ends on the noisy image histogram can be phased out with successive iterations. This serves as an advantage to the proposed histogram-based clustering approach over other existing methods because any FIN noise intensities other than those of I_{min} and I_{max} can also be detected.

At the end of the impulse detection stage, a two-dimensional binary noise map $B^{(t)}(i, j)$ is generated to flag the locations of noise and noise-free pixels. The binary noise map, which has been a trademark for switching filters, is useful in selecting noise-free pixel candidates for restoration. In addition, the binary noise map prevents noise-free pixels from being unnecessarily altered, which is an advantage over the nonswitching counterparts in terms of detail preservation and runtime efficiency. In our proposed algorithm, $B^{(t)}(i, j)$ is formed from the clusters that contain noise-free pixels:

$$B^{(t)}(i, j) = \begin{cases} 0 & : LB \leq x(i, j) \leq HB \wedge I_{pepper} \leq x(i, j) \leq I_{salt} \\ 1 & : \text{otherwise} \end{cases} \quad (14)$$

At the beginning of each iteration, we assume that all of the image pixels are good, i.e., $B^{(t)}(i, j) \equiv 0$. Then, we follow the convention that logic 0's represent the positions of noise-free pixels, and logic 1's represent those of noisy pixels.

3.2. Impulse noise cancellation: locally adaptive fuzzy switching median filter.

According to the switching-scheme framework, the binary noise map $B^{(t)}(i, j)$ acts as a “switch” by invoking the filtering mechanism only when noise pixels are detected. Otherwise, the filtering action is skipped. In this framework, we employ an adaptive switching median filter, called the Locally Adaptive Fuzzy Switching Median (LAFSM), to perform the restoration duties. Here, we provide an in-depth theoretical discussion and analysis on a step-by-step basis in its design and implementation.

The LAFSM filtering algorithm adopts an adaptive size filtering window W_f with $(2K_f + 1) \times (2K_f + 1)$ dimensions, given here as

$$W_f = \{(p, q) \mid -K_f \leq p, q \leq K_f\}, \tag{15}$$

where K_f is a nonzero positive integer. For every noise pixels detected, K_f is initialized to one, i.e., W_f uses a square-shaped filtering window with odd 3×3 dimensions.

The algorithmic description of our LAFSM filtering strategy is summarized as follows:

1. Calculate the number of noise-free pixels in W_f using

$$G_f(i, j) = \sum_{(p,q) \in \Omega_f} \neg B^{(t)}(i + p, j + q) \tag{16}$$

where the operator ‘ \neg ’ denotes negation operation on $B^{(t)}(i + p, j + q)$ and $\Omega_f = \{x(i + p, j + q) \mid (p, q) \in W_f, (p, q) \neq (0, 0)\}$.

2. Iteratively extend W_f outward by one pixel at each of its four sides (i.e., $K_f \leftarrow K_f + 1$) if $G_f(i, j) < 1$. Repeat Steps 1 and 2 until the criterion $G_f(i, j) \geq 1$ is satisfied.
3. Determine the median pixel $M(i, j)$ using all of the noise-free pixels contained in the current window W_f . The median pixel $M(i, j)$ is given as

$$M(i, j) = \text{med}\{x(i + p, j + q) \mid (p, q) \in \Omega_f, B^{(t)}(i + p, j + q) = 0\}. \tag{17}$$

4. Extract the local information $L_i(i, j)$ from the current window W_f according to

$$L_i(i, j) = \max\{|x(i + u, j + v) - x(i, j)| \mid \forall -1 \leq u, v \leq 1\}. \tag{18}$$

5. Determine the fuzzy membership value $F_i(i, j)$ from the extracted local information $L_i(i, j)$

$$F_i(i, j) = \begin{cases} 0.0 & : L_i(i, j) \leq T_1 \\ \frac{L_i(i, j) - T_1}{T_2 - T_1} & : T_1 < L_i(i, j) < T_2, \\ 1.0 & : L_i(i, j) \geq T_2 \end{cases} \tag{19}$$

where T_1 and T_2 are two predefined thresholds.

6. Compute the restoration term $y(i, j)$ as follows:

$$y(i, j) = [1 - F_i(i, j)] \cdot x(i, j) + F_i(i, j) \cdot M(i, j). \tag{20}$$

It is well known that the median is a robust statistical estimator of location [33]. From a statistical standpoint, the median estimator will naturally reach its 50% breakdown point, which means that it remains as a reliable estimator until the number of outliers enclosed in W_f surpasses the 50% limit. Essentially, the LAFSM filtering is not spared from this drawback as experienced by other median-based filters. However, the recursive implementation plays a major role in keeping the median estimator from such a critical situation [33]. Previously restored pixels used for the estimation of currently processed pixels minimize the risk, if there is any, for the number of impulsive pixels to exceed

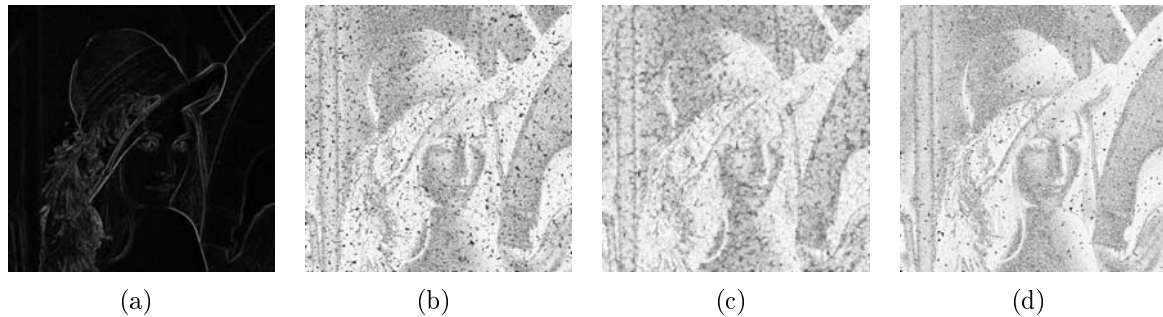


FIGURE 7. Extracted local information L_i from (a) the original “Lena” image, with the image corrupted with 30% of (b) MIX noise, (c) UNIF noise, and (d) SNP noise

half of the total pixels (i.e., $0.5(2K_f + 1)^2$ pixels) in the current filtering window W_f . In addition, the adaptive mechanism employed in LAFSM filtering allows W_f to change its window size according to the local statistics. In that way, we are able to produce higher output correlation and improve the impulse noise suppression capability without blurring the image details.

Although noise-free pixels are relatively easy to select with the aid of the binary noise map $B^{(t)}(i, j)$, choosing the number of noise-free pixels to be used as candidates for restoration poses a challenge. Loss of fine image details and blurring can be introduced into the filtered image if the median pixels used for restoration belong to nonlocal neighbors [13]. For certain regions in images with more impulsive pixels, we want to enlarge the size of W_f ; whereas for certain regions with fewer impulsive pixels, we want to use a smaller window and stop the window expansion process. The key is how to select an appropriate number of noise-free pixels for the restoration process. Therefore, we impose a limit for W_f to contain a minimum number of noise-free pixels, and we choose the limit to be one, as in Step 2 before the window expansion is halted. Note that only a minimum of one noise-free pixel is required for the termination of window expansion because determining the precise number of noise-free pixels is relatively difficult. Similarly, the stopping criteria for window expansion based on local image statistics, e.g., image’s fine details and edges, are complicated because the presence of impulse noise cannot be ignored. However, the rough estimation of the required number of noise-free pixels could be offset by the powerful local information extraction to be done later in our LAFSM filtering algorithm.

In Step 4, the LAFSM filtering algorithm extracts the local information $L_i(i, j)$ from the noisy image using the MAX-operator in (18). The idea of local information extraction means highlighting important image features, i.e., fine image details, thin lines, edges, and textures, even after the image has been degraded by noise. To this end, we propose the use of MAX-operator because it is a fairly simple mathematical concept that possesses powerful abilities to distinguish between noise pixels and image details [1, 17]. Figure 7 illustrates the extracted local information from the original and noisy “Lena” images. From Figure 7(a), the dark regions represent the areas in the original “Lena” image that are composed of homogenous regions with smoothly varying intensities. Conversely, the bright lines indicate image details and edges that have considerably high contrast with their surrounding pixels. The presence of impulse noise results in high absolute deviations between pixels in the noisy images and, thus, significantly increases the overall brightness of the images in Figures 7(b)-7(d). Most of the impulsive pixels are set to occupy the highest intensity whereas the noise-free pixels take on other intensities in the noisy image

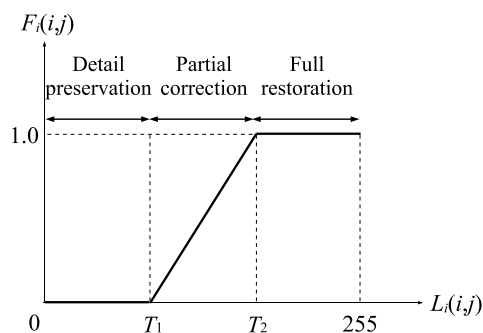


FIGURE 8. Fuzzy membership function of the LAFSM filtering

dynamic range. In essence, the intensity brightness of the extracted local information $L_i(i, j)$ represents the grade of uncertainties present.

In Step 5, the LAFSM filtering algorithm estimates the “fuzziness” of the extracted local information $L_i(i, j)$. Because a noteworthy feature of fuzzy paradigms is its handling of imprecise and conflicting input data [32], fuzzy reasoning is adopted to handle uncertainties that are present in the extracted local information. These uncertainties, e.g., pixels at edges or thin lines being mistaken as noise pixels, are caused by the non-linear statistical characteristics of the impulse noise. Therefore, the fuzzy membership function prescribed in (19) is used to address the imprecision in extracted local information. Furthermore, the function provides a rule base for restoration that emulates the basic sharpening enhancement rules as follows: 1) small changes in intensity should be neutralized, 2) dark regions should remain dark (or possibly darken), and 3) bright regions should maintain bright (or possibly brighten) [44]. The first two rules are achieved through the extracted local information in subdomain $L_i(i, j) \leq T_1$ of (19). The third and last rule is represented by the subdomain $L_i(i, j) \geq T_2$, in which impulsive pixels are smoothed while image sharpness is preserved. Extracted local information in the subdomain $T_1 < L_i(i, j) < T_2$ is adaptively decoded and inferred by (19) on its level of uncertainties. These three subdomains in (19) are graphically illustrated by the three segments in Figure 8. The outcome of the inferencing using the rule base represented by (19) is a numerical fuzzy membership value $F_i(i, j)$ for restoration that articulates linguistic variables such as *detail preservation*, *partial correction*, and *full restoration*.

Subsequently, the fuzzy membership value $F_i(i, j)$ is used to approximate an accurate restoration term $y(i, j)$ in Step 6. The performance of LAFSM filtering depends on the weight provided by $F_i(i, j)$. Instead of crisply replacing the noise pixel $x(i, j)$ with the median pixel $M(i, j)$, as practiced by switching median filters [7-10, 12-16, 18-22], $F_i(i, j)$ determines whether more of $x(i, j)$ or $M(i, j)$ is restored during the LAFSM filtering. Generally, Step 5 complements Step 6 by providing it with a means for “soft-switching”. It is this mechanism of the LAFSM filtering that allows it to adapt to a wide variation in impulse noise densities. Correspondingly, the newly restored pixel $y(i, j)$ is used for clustering in the detection action of the subsequent adjacent pixels. As a result, the image details are very well preserved after restoration.

3.3. Stopping criteria for iteration. Many of the iterative filtering schemes available [18, 19, 22] take a relatively long runtime to converge, and the convergence point is usually not the best restoration for the filtered image. For simplicity, the filters found in the literature fix the number of iterations 1) according to the empirical observations made on a small subset of test images [20, 21] or 2) based on the impulse noise densities [28, 34]. Fixing the number of iterations cannot yield optimal filtering performance for

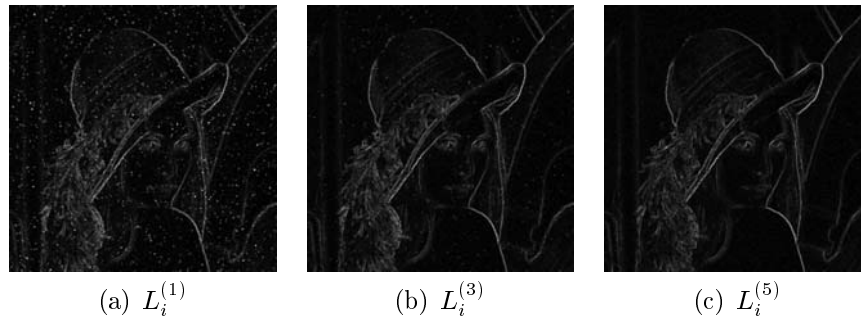


FIGURE 9. Evolution of the extracted local information as the number of iteration increases. Extracted local information of the filtered “Lena” images after the (a) first, (b) third, and (c) fifth iteration. The “Lena” image is originally contaminated with 30% MIX noise. Note that impulses are successively removed after each iteration without degrading fine image details.

two reasons. First, different images have different image contents and global statistics; thus, they require different numbers of iterations, even when they are corrupted with the same density of impulse noise. Second, impulse noise density is not known *a priori* in real-world applications. For these reasons, filters that are iterative in nature should attempt to automate their iterative stopping criteria based on image information (e.g., noise contents and image details) in the simplest manner possible.

The impulse detection and cancellation algorithms of the AVSHC filter are iteratively performed until the stopping criteria, to be developed in this section, are satisfied. In this framework, we introduce a no-reference image “roughness” index, called the Normalized Local Information (NLI), to estimate the image contents and noise levels in the filtered image. The NLI index provides a quantitative measure of the true image content (i.e., sharpness and contrast as manifested in visually salient geometric features such as edges and textures) in the presence of noise. To achieve fast runtime for feasible implementation, we do not wish to introduce any lengthy computation involving complex mathematical formulations. As a rule, we strive for a simple stopping criterion by using the information already available from previous processes. Therefore, the NLI roughness index for the filtered image is computed as an extension of the local information extraction in (18) using

$$\varphi^{(t)} = \sum_{i=0}^{M-1} \sum_{j=0}^{N-1} \left[\frac{L_i^{(t)}(i, j)}{M \cdot N} \right], \quad (21)$$

where $L_i^{(t)}$ and $\varphi^{(t)}$ denote the extracted local information for a pixel at location (i, j) and the NLI roughness index, respectively, in the t th iteration. Because iterations should be halted when the noise pixels are almost eliminated, the impulse detection and cancellation operations are discontinued when the difference between two consecutive NLI roughness indices $|\varphi^{(t)} - \varphi^{(t-1)}|$ is small. To restate this stopping criterion more concisely, the impulse detection and cancellation operations are stopped when the first local minimum is found, i.e.,

$$\frac{d}{d\varphi} (|\varphi^{(t)} - \varphi^{(t-1)}|) = 0, \quad (22)$$

where $\varphi^{(0)} = 0.0$.

At each iteration, we apply the adaptive threshold $F_2^{(t)}$ in (8) as a decreasing function of

$$F_2^{(t)} = F_2^{(t-1)} - 50 \quad (23)$$

to ensure high accuracy in impulse detection. Figure 9 shows the extracted local information of filtered “Lena” images with increasing numbers of iterations. Note that the number of small patches, which indicate the remaining impulsive pixels, is successively reduced with increasing iterations. The decreasing impulse noise densities after each iteration justify the lowering of $F_2^{(t)}$. Together, $F_1^{(t)}$ and $F_2^{(t)}$ are used to control the tradeoff between the degree of detail preservation and the sensitivity of impulse detection, respectively. The manner in which $F_2^{(t)}$ decreases is crucial because it can affect the NLI roughness index in the later stage and, therefore, jeopardize the determination of the optimal number of iterations. At early iterations when the impulsive pixels are still abundant in the noisy image, the proposed impulse detectors identify only the pixels that are likely to be noise candidates with the large $F_2^{(t)}$ threshold. Then, we decrease $F_2^{(t)}$ in the subsequent iterations to further scrutinize impulsive pixels disguising as “noise-free” pixels near fine image details that are much more difficult to identify.

Generally speaking, the NLI roughness index gives a rough estimation of the remaining noise content and detail degradation after each iteration. For example, the more impulsive pixels that are swarming the homogeneous regions in the filtered image, the greater the NLI roughness index becomes. As the number of iteration increases, the NLI roughness index diminishes and eventually reaches a steady state when only nonremovable image details contribute to the index. To support these claims, we performed an experiment to investigate the changing trend of $|\varphi^{(t)} - \varphi^{(t-1)}|$ and the effect of varying $F_2^{(t)}$ with increasing iterations. In this experiment, we added 5%, 25%, and 50% of MIX noise into the set of 10 standard test images. Each noisy test image is filtered using the AVSHC filter with 10 iterations (i.e., $1 \leq t \leq 10$), and this process is repeated for fixed $F_2^{(t)} = 50$, $F_2^{(t)} = 250$, and adaptive $F_2^{(t)}$, as defined in (23). For reasons that will become apparent in the following section, we set the remaining parameters as $K_d = 1$, $F_1^{(t)} = 10$, $T_c = 50$, $T_1 = 10$, and $T_2 = 50$ throughout this experiment⁵. Plots of the experimental results are given in Figure 10. The NLI difference between two consecutive iterations is recorded, and the average NLI difference from the set of 10 noisy images is plotted with varying iterations. For the sake of completeness, we also use the mean-squared error (MSE) metric to test the restoration performance of the AVSHC filter with growing numbers of iterations, i.e., the MSE from each iteration is recorded and then averaged. We observe that our proposed NLI index consistently terminates the iterations at different impulse noise strengths when the lowest MSE values are attained. The behavior of the NLI index not only provides an optimized iteration number but also tends to reveal advantageous and interesting behavioral characteristics of the AVSHC algorithm to which it is applied in a completely unsupervised fashion and without access to a reference image or an estimate of the MSE. As a case in point, the NLI difference decreases drastically after the first few iterations, indicating that most of the impulses are removed, and then it rises slightly in the subsequent iterations because of the unnecessary removal of fine image details. This phenomenon is observed most strongly in the experiments with 5%

⁵For the case of adaptive $F_2^{(t)}$, it is worth noting that the initial condition is set as $F_2^{(0)} = 250$. As the number of iterations t increases, the condition $F_2^{(t)} \leq F_1^{(t)}$ will be developed when $t > 5$, in which (8) will be violated. For (8) to hold true, the condition $F_2^{(t)} > F_1^{(t)}$ must be satisfied, and hence, an additional condition $F_2^{(t)} \geq 50$ is imposed for $t > 5$. Further discussion of the choice of parameters is presented in Section IV-A.

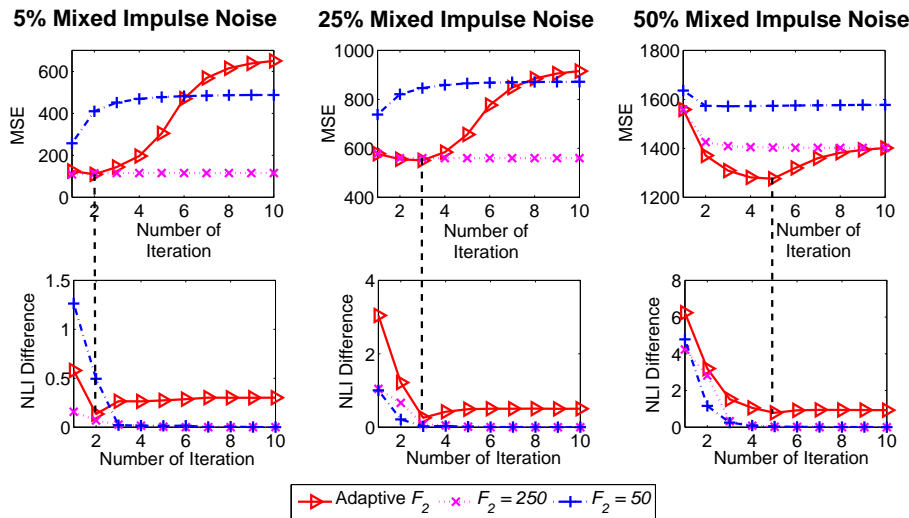


FIGURE 10. The no-reference NLI index as an estimate of the MSE. The NLI difference and MSE are averaged from 10 noisy test images and then plotted as a function of iteration for different choices of $F_2^{(t)}$.

and 25% noise densities. Furthermore, we observe that varying the $F_2^{(t)}$ parameter renders a more accurate and smooth termination of iteration than using a fixed $F_2^{(t)}$.

In general, the proposed iterative stopping criterion based on the NLI roughness index can achieve satisfactory results after two iterations. However, we want our stopping criterion to end the iterations neither too early nor too late for any level of impulse noise densities. Insufficient numbers of iterations often indicate unfiltered noise patches in the filtered image [43]. Fortunately, our proposed stopping criterion can restrain this problem by employing (22). However, stopping the iterations too late can cause blurring, and each additional iteration increases the computational cost significantly. From the simulation results in Figure 10, we set an additional terminal point to the stopping criterion for operations to end at a maximum of five iterations (i.e., $1 \leq t \leq 5$) if the convergence requires more than five iterations before the difference between the successive NLI roughness indices can reach a steady state bounded by (22). This additional termination criterion is also effective to avoid stopping the iterations too late. As is demonstrated in the next section, the AVSHC filter shows excellent restoration results with a relatively fast runtime.

4. Simulation Results and Discussions. In this section, we evaluate the performance of our proposed AVSHC filter using the 10 aforementioned 8-bit monochrome standard test images 512×512 in size. Each of the test images is superimposed on the MIX, UNIF, and SNP noise for noise densities ranging from 5% to 50% in 5% noise steps. For comparison, the noisy images are also restored using several well-known impulse noise filters. These state-of-the-art methods are the switching-bilateral (SB) [13], directional weighted-median (DWM) [18], contrast enhancement-based (CE) [20], robust impulse noise variance estimation (RINVE) [21], new adaptive switching median (ASWM) [22], functional minimization effective median (FMEM) [28], genetic programming (GP) [33], triangular-based linear interpolation with differential evolution (TLIDE) [34], and adaptive kernel-based semi-parametric regularization (KASPR) [42] filters. These methods also represent the wide array of approaches used to address impulse noise filtering problems in the current literature.

Some of the filters mentioned above work with a number of tuning parameters. In our simulation, we used the parameter values as suggested in the corresponding references, as follows. For SB, $N = 2$, $\rho = 40$, $\sigma_S = 2$, $\sigma_R = 40$, $[Tk_1, Tk_2] = [30, 15]$ for SNP noise removal, and $[Tk_1, Tk_2] = [25, 5]$ for UNIF and MIX noise filtering. For DWM, $w_m = 2$, $T_0 = 510$, $N_{\max} = [5, 10]$, and window size is 5×5 . For CE, K is initialized as $K = 1$ and varied as $K = K + t$ where $t = (10, 15, 20, 25, 30)$; a 3×3 window is used when the impulse noise density is below 40% and a 5×5 window otherwise. For ASWM, $L = 1$, $\delta = 0.1$, $\epsilon = 0.01$, $\alpha_0 = 20$, and $\alpha_{n+1} = 0.8\alpha_n$ for $n \geq 0$. For FMEM, $[\delta_0, \delta_1, \delta_2, \delta_3] = [40, 25, 10, 5]$, $r_{\max} = 3$, and $s = 0.6$ for noise density greater than 30%, and $s = 0.1$ otherwise. For GP, $\alpha = \frac{1}{3}$, $\omega = 5$, and a 3×3 window is used for filtering. For TLIDE, $t_1 = 5$, $t_2 = 10$, $t_3 = 3$, $a = 0.030$, $b = -0.589$, $\delta = -0.155$, τ employs a 32×32 non-overlapping $\Omega(i, j)$ block, and detection window size of 5×5 is used for impulse noise density estimation; [Sliding window sizes, t_3] are $[3 \times 3$ -to- 11×11 , 1-to-29] and $[5 \times 5$ -to- 13×13 , 3-to-28] for the first and second epochs, respectively, and $[t_1, t_2] = [0$ -to- 13 , 12-to-25] for the tuning parameters. For KASPR, $L = 6$, $\vec{\mu} = (0.01, 0.1, 0.5, 5, 50, 100)$, $\vec{\mu}_2 = (0, 0, 0, 0.1, 1, 3)$, $\vec{m} = (2, 2, 1, 1, 1, 0)$, $\vec{s} = (3, 3, 1)$, $\mu_0 = 0.1$, $\nu = 3$, $\lambda = 1$, $\sigma = 3$, and $\vec{c} = (1, 1, 1, 1, 1, 1)$, vector \vec{N} takes the values $(5, 5, 5, 5, 5, 5)$, $(5, 5, 5, 7, 7, 7)$, $(7, 7, 7, 7, 7, 7)$, $(7, 7, 7, 9, 9, 9)$ whereas \vec{p} is $(0.1, 0.1, 0.1, 0.1, 0.2, 0.2)$ for images with a medium number of edges and $(0.2, 0.2, 0.1, 0.1, 0.2, 0.4)$ for images that contain many edges. However, it should be noted that some of these values need to be heuristically modified, depending on the image contents, to obtain the best restoration for fair comparison.

4.1. Selection of parameters. The AVSHC filter is implemented according to the system architecture as shown in Figure 1. Noisy image is processed in a raster-scan fashion, i.e., every pixel is scanned row-by-row from the top-left corner to the bottom-right corner of the noisy image. The LAFSM filtering is invoked when a pixel is identified as noise by the impulse detectors. Additional iterations are performed only if the filtered image does not satisfy the stopping criteria for iteration as defined in Section 3.3.

From extensive simulations, we empirically determined the threshold values for the parameters used by the proposed AVSHC filter. We used the MSE metric to select the optimal values for the parameters. The MSE, defined as

$$\text{MSE} = \frac{\sum_{i=0}^{M-1} \sum_{j=0}^{N-1} [y(i, j) - o(i, j)]^2}{M \cdot N}, \quad (24)$$

quantitatively measures the error that occurs if we use y as an approximate for o at pixel location (i, j) . Hence, we seek the set of parameter values that can produce the lowest MSE for optimal performance of the AVSHC filter.

In impulse denoising applications, the question of selecting optimal parameter values has not been fully answered from a theoretical perspective. As noted in [13], parameters employed in the impulse detection stage have a more significant impact on the restoration performance of the switching-based filter than those used in the impulse cancellation stage. Because the proposed AVSHC filter is a switching-based filter, its restoration performance is very dependent on the impulse detectors. In this respect, the K_d parameter controlling the size of the detection window $W_d(i, j)$ and the clustering threshold T_c play important roles in the overall performance of the AVSHC filter. Similarly, the remaining two parameters, $F_1^{(t)}$ and $F_2^{(t)}$, engaged in the impulse detection stage determine the optimal number of iterations and, thus, avoid the unnecessary removal of image fine details that could lead to blurring of the filtered image. However, the T_1 and T_2 parameters for the impulse filtering process assist in the sharpness preserving ability of the AVSHC filter. The choice of T_1 and T_2 is robust and does not significantly affect the quality of the filtered

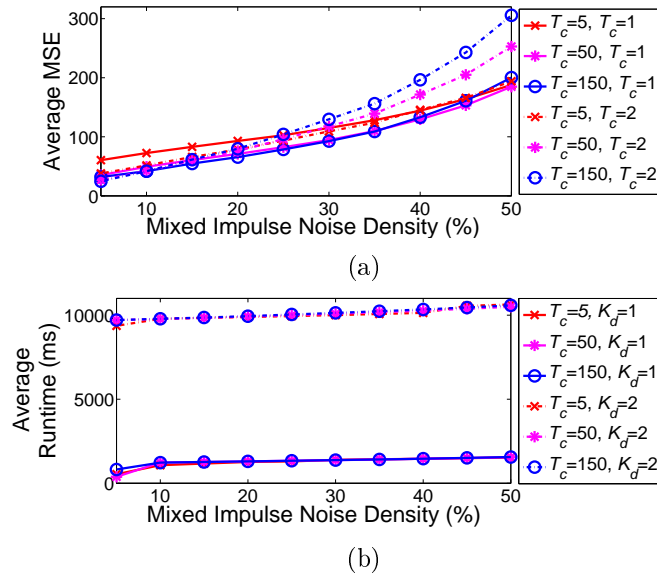


FIGURE 11. Selection of K_d and T_c parameters based on the MSE metric and runtime

image. The behaviors of these parameters are well understood, and we refer the reader to our previous work in [1] for detailed discussion of T_1 and T_2 .

To begin, we set up an experiment to investigate the effect of changing K_d and T_c across various impulse noise densities. In this experiment, we test the restoration ability and the runtime consumption of the AVSHC filter using various combinations of K_d and T_c . We then run the AVSHC filter by fixing $K_d = 1$ while varying $T_c = (5, 50, 150)$, and we repeat this process with $K_d = 2$. On the basis of the outcome of earlier experiments, as shown in Figure 10, we select $F_1^{(t)} = 10$, $F_2^{(0)} = 250$, $T_1 = 10$, and $T_2 = 50$. The set of 10 standard test images, each corrupted with 5 to 50% of MIX noise in 5% noise steps, is used in this experiment. The MSE and runtime obtained in the simulation are averaged and plotted against the MIX noise densities, and the plots are shown in Figure 11. The selection of K_d and T_c is fairly simple because the performance of the AVSHC filter is tightly bounded with minimal difference in MSE when T_c lies in a wide range [5, 150]. Examining the plot in Figure 11(b), we choose $K_d = 1$ instead of $K_d = 2$ to minimize the runtime taken by the AVSHC filter without any significant detrimental effect on restoration.

Next, we analyze the effects of $F_1^{(t)}$ and $F_2^{(t)}$ on the restoration performance of the AVSHC filter. From extensive simulations, we have elected to conserve space in this presentation, and thus, do not include the redundant simulations for $F_1^{(t)}$. We found that the performance of the AVSHC filter is not dependent on the $F_1^{(t)}$ parameter as long as the condition $F_1^{(t)} < F_2^{(t)}$ is satisfied, which is also a mathematical condition for (8) to be valid. We focus on the selection of $F_2^{(t)}$, and Figure 10 shows the effects on the average MSE and NLI values using fixed and varying $F_2^{(t)}$'s. A large $F_2^{(t)}$ is more favorable than a smaller $F_2^{(t)}$ because larger values (i.e., $F_2^{(t)} > 150$) ensure the removal of impulses that include some image fine details. Conversely, smaller $F_2^{(t)}$ values may retain some impulses while keeping the fine details of the uncorrupted image intact in the filtered image. This justifies the higher MSE values, which correspond to the presence of impulses when a smaller $F_2^{(t)}$ is used. These observations allow us to achieve optimal performance for the AVSHC filter by decreasing the $F_2^{(t)}$ value after each iteration, as dictated by (23). A strategy such as this will aggressively remove impulses that present during the first few

TABLE 1. Impulse classification ratio

Mixed Impulse (MIX) Noise					
Methods	10%	20%	30%	40%	50%
SB [13]	94.2593%	93.5416%	92.4933%	91.6965%	90.7276%
DWM [18]	96.9735%	93.9974%	87.4331%	81.6935%	72.5556%
RINVE [21]	94.6107%	94.2894%	92.4951%	89.8740%	90.3767%
GP [33]	94.9380%	94.2533%	93.5368%	92.7556%	91.7816%
KASPR [42]	24.9438%	29.4550%	35.9226%	44.4183%	52.7861%
AVSHC	97.9735%	95.9925%	94.6682%	93.5786%	93.0097%
Uniform Impulse (UNIF) Noise					
Methods	10%	20%	30%	40%	50%
SB [13]	93.1590%	91.4258%	89.6313%	87.5417%	84.9315%
DWM [18]	95.9537%	92.3431%	87.9035%	83.7352%	76.8979%
RINVE [21]	96.7526%	92.6450%	89.8975%	87.6937%	87.3658%
GP [33]	94.3759%	93.0823%	91.6686%	90.0738%	87.8980%
KASPR [42]	24.3616%	28.5599%	34.9993%	43.4948%	52.0448%
AVSHC	97.6046%	95.8053%	93.6806%	91.4118%	89.1572%
Salt-and-Pepper (SNP) Noise					
Methods	10%	20%	30%	40%	50%
SB [13]	96.2663%	96.2815%	96.3096%	96.3236%	96.3115%
DWM [18]	97.6942%	94.1643%	83.6273%	74.7181%	63.9815%
RINVE [21]	97.1581%	95.6141%	93.7031%	89.0645%	88.0760%
GP [33]	95.4975%	95.3506%	95.1837%	94.9023%	94.1219%
KASPR [42]	24.1121%	28.7113%	31.8078%	44.2901%	52.3459%
AVSHC	98.9052%	98.4784%	98.0928%	97.6023%	97.2830%

iterations with larger $F_2^{(t)}$, before subsequent iterations with decaying $F_2^{(t)}$ scrutinize the detection of impulses that are more difficult to identify. As a result, we successfully deliver a detail-preserving AVSHC filter for effective image restoration.

Additionally, extensive simulations suggest that $K_d = 1$, $T_c = 50$, $F_1^{(t)} = 10$, $F_2^{(0)} = 250$, $T_1 = 10$, and $T_2 = 50$ could yield excellent restoration results, both qualitatively and quantitatively. Therefore, this set of parameter values is used in the remaining simulations to develop the main results for comparison with other impulse noise filters. Note that this set of values is robust, and thus, it appears advantageous to our proposed method in the sense that it does not need further modifications when applied to any images corrupted with a wide variation of impulse noise densities. Intuitively, the performance of the AVSHC filter can be further improved if the parameters can be made locally adaptive, i.e., if they can be fine-tuned to remove precise amounts of impulse noise present in the detection window. Unfortunately, such an ideal solution would be time consuming, and the best way to fine-tune the parameters is not immediately known.

4.2. Impulse detection performance. To appreciate the effectiveness of the proposed impulse detector, we first demonstrate the impulse detection performance of our AVSHC filter. The real power of the proposed AVSHC filter is revealed in Tables 1 and 2, which list the average impulse classification and detection ratios, respectively, from 10 standard test images. The impulse classification ratio is defined as the number of correctly identified pixels (i.e., the sum of the correctly detected impulses and the noise-free pixels), divided by the total number of pixels in the image. Then, the impulse detection ratio represents the number of detected impulses divided by the total number of impulses. Consequently, a good impulse detector should be able to accomplish greater classification and detection

TABLE 2. Impulse detection ratio

Mixed Impulse (MIX) Noise					
Methods	10%	20%	30%	40%	50%
SB [13]	89.2515%	89.0440%	88.9730%	88.8681%	88.6098%
DWM [18]	82.7296%	82.5717%	88.0129%	89.2414%	94.0920%
RINVE [21]	89.0322%	88.5840%	87.3573%	92.0469%	92.9268%
GP [33]	91.9303%	92.0090%	91.9711%	91.7583%	91.3783%
KASPR [42]	99.6795%	99.7154%	99.7410%	99.7383%	99.7381%
AVSHC	98.4002%	97.9928%	97.6891%	97.4911%	97.2881%
Uniform Impulse (UNIF) Noise					
Methods	10%	20%	30%	40%	50%
SB [13]	79.8180%	79.5961%	79.4344%	79.0596%	78.4005%
DWM [18]	69.4603%	69.2360%	77.3089%	79.2271%	87.7817%
RINVE [21]	78.4272%	76.3152%	76.8840%	85.5316%	87.1314%
GP [33]	86.1804%	86.2233%	85.9802%	85.6050%	84.7283%
KASPR [42]	99.3752%	99.3977%	99.4644%	99.4563%	99.4496%
AVSHC	98.6348%	97.9981%	97.7521%	97.5488%	97.2845%
Salt-and-Pepper (SNP) Noise					
Methods	10%	20%	30%	40%	50%
SB [13]	97.6161%	97.5622%	97.5349%	97.5243%	97.4222%
DWM [18]	93.9857%	91.7035%	92.8547%	90.4002%	91.3965%
RINVE [21]	96.9710%	97.2430%	95.9838%	97.7319%	97.1115%
GP [33]	77.0493%	97.5646%	97.4085%	96.9915%	95.8811%
KASPR [42]	99.9919%	99.9953%	99.9977%	99.9975%	99.9982%
AVSHC	100.000%	100.000%	100.000%	100.000%	100.000%

ratios for high accuracy impulse detection. In Tables 1 and 2, we use a bold-face font to highlight the highest ratio in each column.

It can be seen that our proposed impulse detector has the highest average classification rates for all three impulse noise models simulated compared with the KASPR filter in Table 1. However, the KASPR filter has higher average impulse detection rates than our AVSHC filter for the MIX and UNIF noise models in Table 2. Nevertheless, our proposed impulse detection scheme records a clean 100% average detection rate for the SNP noise model. The higher average impulse detection rates, coupled with low impulse classification rates, suggest that the KASPR filter made a number of false impulse detections, and thus, more noise-free pixels were misclassified as impulsive pixels. In fact, if we regard the total errors produced by an impulse detector as the sum of missed detections and false detections, our proposed AVSHC detection yields the lowest average errors for all types of impulse noise models, as shown in Figure 12. We further note that the switching filters generally have lower average errors in impulse detection than the nonswitching KASPR filter. Among the switching filters, our AVSHC filter, which employs signal augmentation has higher impulse detection rates than filters without signal augmentation (e.g., SB, DWM, RINVE, and GP filters).

4.3. Comparison in image restoration. The performances of all filters are evaluated qualitatively through visual inspection and quantitatively by using the peak signal-to-noise ratio (PSNR), defined as

$$\text{PSNR} = 10 \log \left(\frac{I_{\max}^2}{\text{MSE}} \right). \quad (25)$$

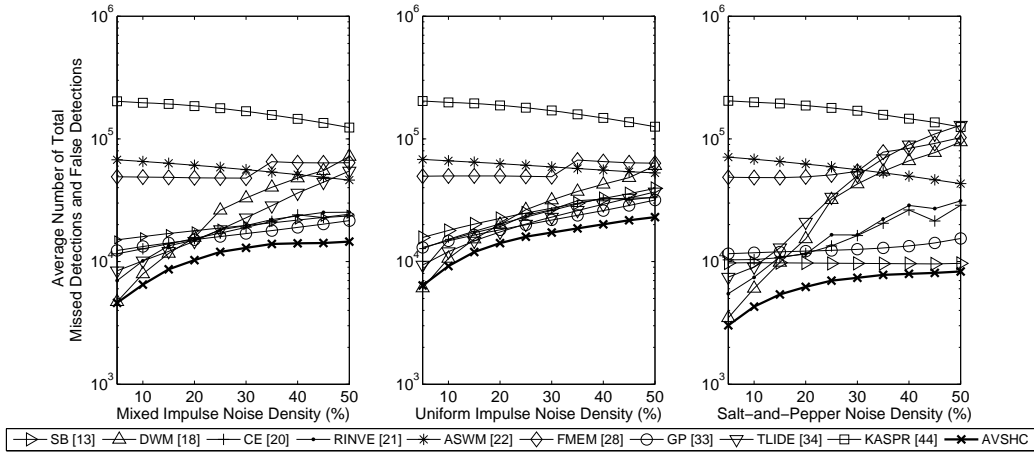


FIGURE 12. Sum of missed detections and false detections of pixels; graphs plotted as the average errors from 10 standard test images versus impulse noise density for the MIX noise (left column), UNIF noise (center column), and SNP noise (right column) models

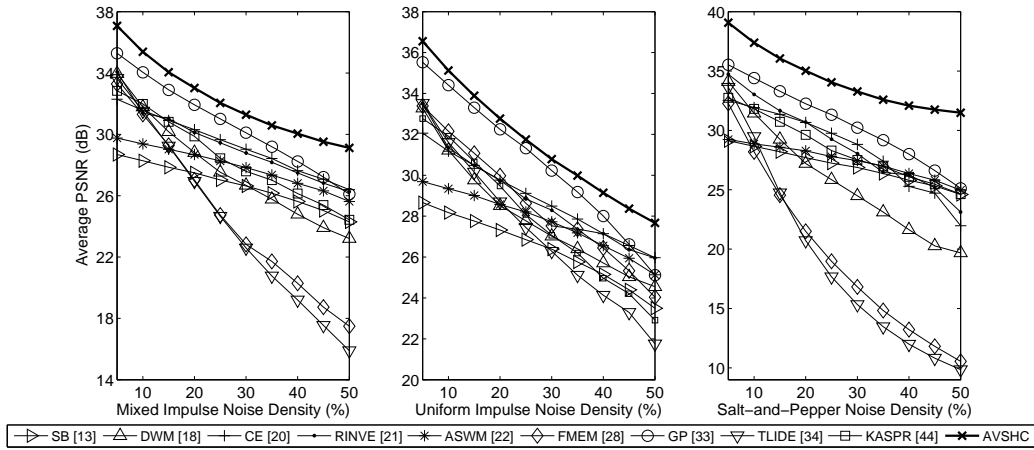


FIGURE 13. The graphs of average PSNR (dB) versus impulse noise density for MIX noise (left column), UNIF noise (center column), and SNP noise (right column)

The PSNR assessment is used for measuring the differences and similarities between the original and restored images [45]. In terms of detail preservation, the PSNR by itself cannot directly measure any underlying information such as fine image details because different combinations of image distortion and residual impulse noise can offset the effects of one another [46]. As a remedy, we have chosen the mean absolute error (MAE) assessment to account for the detail-preserving characteristics of filters implemented. The MAE is given as

$$MAE = \frac{\sum_{i=0}^{M-1} \sum_{j=0}^{N-1} |y(i, j) - o(i, j)|}{M \cdot N} \tag{26}$$

For the MAE assessment scheme, smaller MAE value indicates better detail preservation in the restored image. In contrast, greater PSNR value signifies better noise suppression in image restoration.

We plot the graphs of average PSNR and MAE versus impulse noise density in Figures 13 and 14, respectively, for simulations using the MIX, UNIF, and SNP noise models.

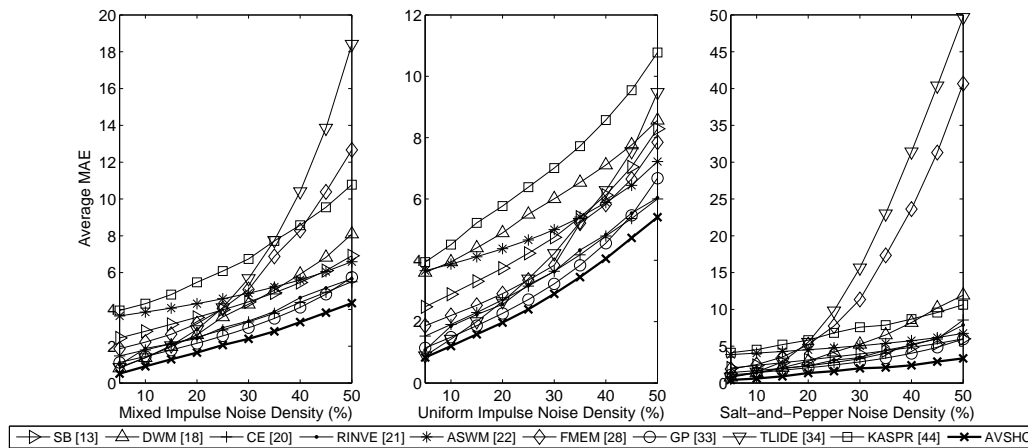


FIGURE 14. The graphs of average MAE versus impulse noise density for MIX noise (left column), UNIF noise (center column), and SNP noise (right column)

Obviously, our AVSHC filter achieves significant improvement over other filters in terms of average PSNR and MAE. The higher average PSNR values and relatively lower average MAE values of the proposed filter clearly indicate the ability of the AVSHC filter to process only the impulsive pixels in the noisy image while leaving the uncorrupted pixels unchanged. Regarding visual comparison, Figure 15 displays the subjective visual qualities of the filtered “Lena” images initially corrupted with 50% of MIX noise. It is clearly seen that our AVSHC filter produces the most appealing visual result by successfully suppressing impulses and preserving image details. The filtered image using our proposed AVSHC filter in Figure 15(l) remains sharp, and the edges are not smeared. The difference in detail preservation between other filters and our AVSHC filter can be easily observed by carefully comparing the appearance of the eyes and the face of the woman and the feathers on her hat.

To demonstrate the universality of the proposed AVSHC filter in removing different types of impulse noise models, simulation results for the enlarged portion of the filtered “Baboon” images previously contaminated with 50% UNIF noise are shown in Figure 16. Figure 17 presents the enlarged portion of the corresponding results for the filtered “Boat” images formerly degraded with 50% SNP noise. These images were chosen specifically because they are rich in details and textures. From Figures 16(l) and 17(l), we observed that the proposed AVSHC filter consistently exhibits excellent impulse attenuation performance. Loss of fine image details is negligible, and subjective sensations are very well reconstructed in the filtered images. The UNIF noise filtering results in Figure 16 show that only the GP filter yields competitive results (in terms of PSNR and MAE). However, the zoomed portion of the filtered image in Figure 16(k) shows that some noise blotches are easily visible. Furthermore, it is obvious that the proposed AVSHC filter produces much better edge preservation when the dark-colored nose and the brightly colored cheek of the animal in Figure 16(l) are examined. In case of SNP noise filtering, the ASWM filter in Figure 17(f) cleanly removes visible impulsive pixels but at the expense of the image fine details. However, the AVSHC filter exhibits better restoration results than the others, as its filtered image in Figure 17(l) is almost indistinguishable from the original input image in Figure 17(a).

When comparing the simulation results in Figures 15-17, we found that our AVSHC filter clearly outperforms other filters regarding the cancellation of impulse noise and preservation of image details. It is also interesting to note that some filters perform

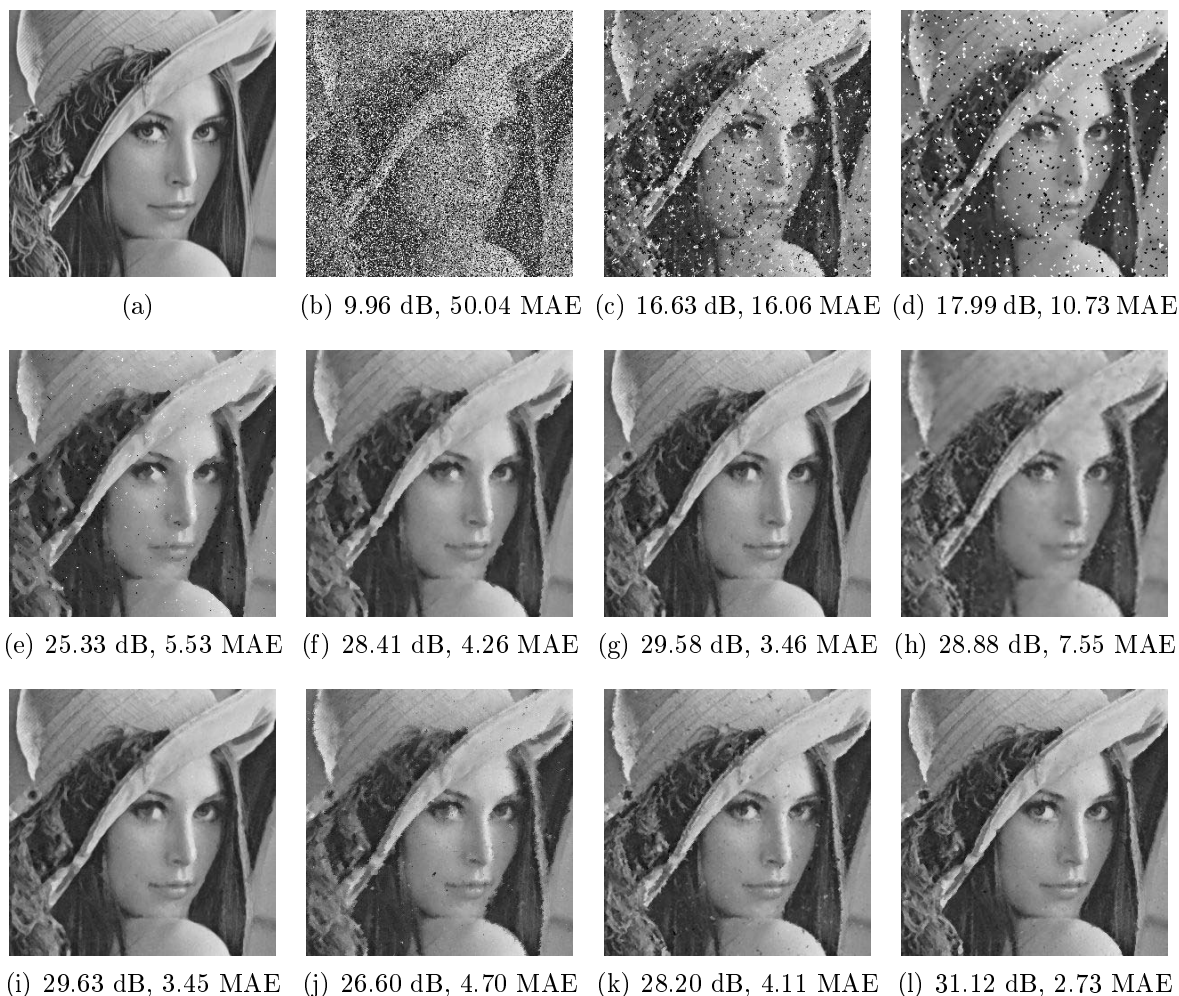


FIGURE 15. (a) A portion of original “Lena” image. (b) Cropped “Lena” image corrupted with 50% MIX noise. Filtered “Lena” images using: (c) TLIDE [34], (d) FMEM [28], (e) DWM [18], (f) ASWM [22], (g) CE [20], (h) KASPR [42], (i) RINVE [21], (j) SB [13], (k) GP [33], and (l) proposed AVSHC filters.

differently, depending on the impulse noise type and density. Although the selection of parameters for the AVSHC filter is based on the MIX noise model, our proposed AVSHC filter performs well over a wide range of impulse noise densities, regardless of the impulse noise models tested. The success behind such performance delivery is mainly attributed to the high accuracy impulse detection, together with the effective restoration scheme, of the AVSHC filter.

4.4. Runtime efficiency. In the following analysis, we compare the runtime of our AVSHC filter with those of other filters implemented in this framework. All of the algorithms are written in C and MATLAB, and runtime simulations are conducted using a Dell laptop with 1.66-GHz Centrino Duo Processor. Figure 18 graphically illustrates the average runtime (in milliseconds, or ms) calculated from 10 standard test images versus impulse noise density for MIX, UNIF, and SNP noise models. On average, the KASPR filter consumes the highest runtime, with a minimum of 1.2×10^6 ms per image execution.⁶

⁶The curves for the KASPR filter are omitted to avoid impinging the ‘Average Runtime’ graph scales in Figure 18.

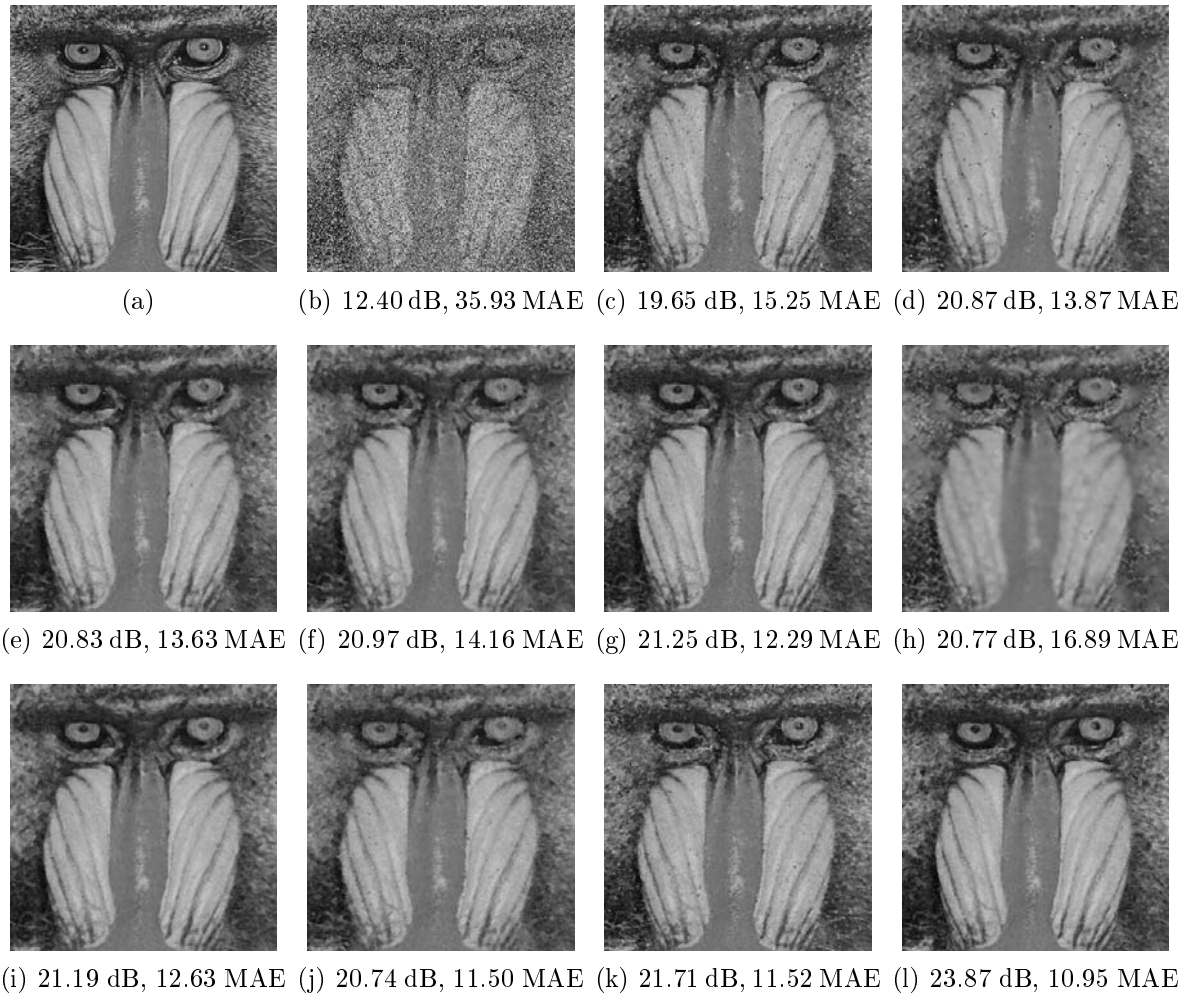


FIGURE 16. (a) A portion of original “Baboon” image. (b) Cropped “Baboon” image corrupted with 50% UNIF noise. Filtered “Baboon” images using: (c) TLIDE [34], (d) FMEM [28], (e) DWM [18], (f) ASWM [22], (g) CE [20], (h) KASPR [42], (i) RINVE [21], (j) SB [13], (k) GP [33], and (l) proposed AVSHC filters.

Despite being an iterative filtering algorithm, our AVSHC filter consumes a relatively low runtime because the proposed filter employs a small 3×3 detection window throughout the detection stage. In addition, our strategy to minimize the computational load in the AVSHC filter’s design contributes to the relatively fast processing time. Generally, the number of iterations required by the proposed filter does not exceed five iterations as bounded by one of the proposed iterative stopping criteria, and the runtime is less than 1.1 s on average per image execution.

5. Conclusion. In this paper, we presented a novel two-stage method for impulse noise reduction based on a switching-scheme concept. The proposed AVSHC filter is applied recursively in iterative manners. In the first stage, an impulse detector inspired by a two-level clustering procedure is used to segregate noise-free pixels into a single cluster. If the center pixel belongs to the cluster containing noise-free pixels, then it is left unchanged. Otherwise, the second stage is invoked to restore any detected noise pixels using an adaptive switching median filter that uses the local information from the surrounding neighborhood. Fuzzy reasoning is exploited as part of the detection and filtering

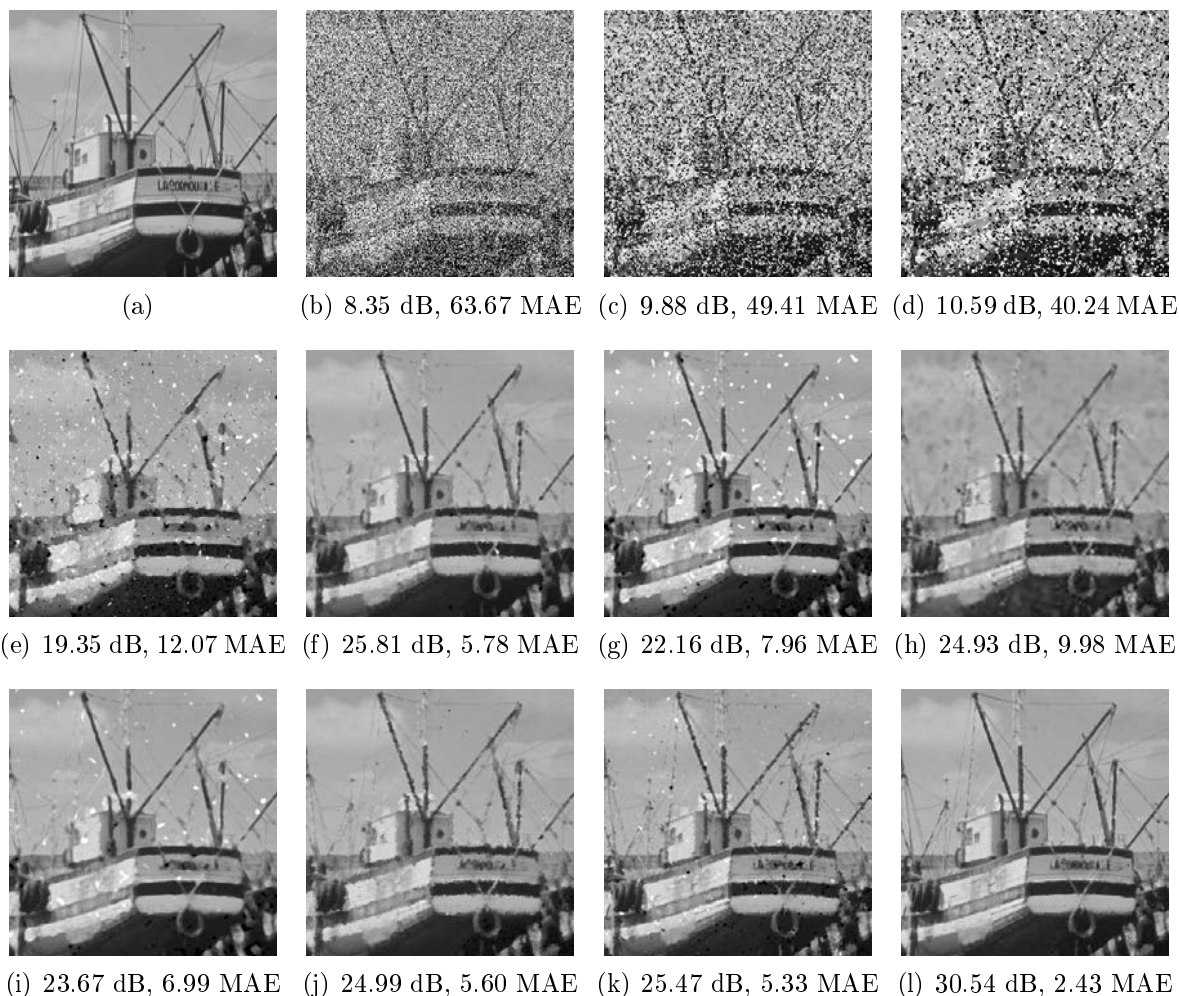


FIGURE 17. (a) A portion of original “Boat” image. (b) Cropped “Boat” image corrupted with 50% SNP noise. Filtered “Boat” images using: (c) TLIDE [34], (d) FMEM [28], (e) DWM [18], (f) ASWM [22], (g) CE [20], (h) KASPR [42], (i) RINVE [21], (j) SB [13], (k) GP [33], and (l) proposed AVSHC filters.

mechanisms to handle the uncertainties present in image data. In addition to the major contribution of this work, which is a clustering-based approach for impulse detection, we introduced a fairly simple no-reference roughness index for measuring noise levels and image contents in a filtered image. From this roughness index, we then proposed stopping criteria to determine the optimal number of iterations. Furthermore, we studied the behavior of the parameters used in our framework through a series of experiments before we empirically tuned these parameters for optimal restoration performance.

One of the attractive properties of the AVSHC filter is its ability to accurately suppress impulse noise while minimizing the destruction of a clean portion of pixels, including fine image details and textures. Moreover, AVSHC can be considered a universal impulse noise filter because of its capability to remove different types of impulse noise models that are commonly encountered in practical cases. This universal behavior gives the AVSHC filter a competitive advantage over many impulse noise filters. Extensive simulation results verify the excellent impulse detection and restoration performances of the filter, both visually and quantitatively, over other filters. The relatively fast runtime and simplicity in implementation can be seen as tremendous advantages that contribute to

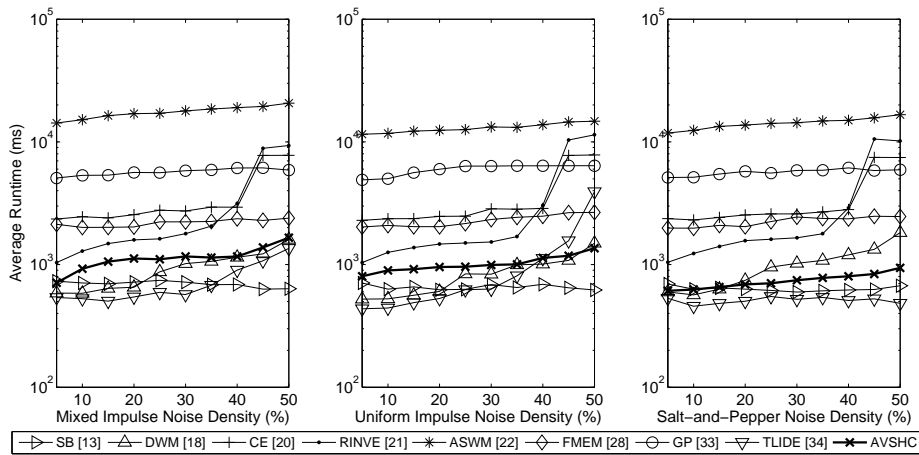


FIGURE 18. The graphs of average runtime (ms) corresponding to various impulse noise densities for MIX noise (left column), UNIF noise (center column), and SNP noise (right column)

the feasibility of the AVSHC filter. In conclusion, the AVSHC filter offers a good tradeoff between computational complexity and image restoration performance for practical image applications.

In our framework, the performance of the proposed method is dependent on a set of parameters, and it is necessary to carefully select the values for the parameters that are used. This necessity is undesirable, and our ongoing research aims at addressing this issue. In this regard, we foresee the attempt to cast our framework into a nonparametric approach may reduce the number of parameters used. Although our proposed method already has a fast runtime, it should be noted that the runtime of our method can be further improved. The implementation of the proposed AVSHC filter can be easily parallelized to take advantage of modern processors with multiple cores. This is possible because the proposed impulse detectors, namely, the augmented variational series and histogram-based clustering, are performed independently for each pixel before their outcomes are combined and evaluated. The use of other unsupervised clustering algorithms to effectively segment pixels according to local image features can be considered as well. Going forward, we envision extending the clustering approach based on signal augmentation to other image denoising problems, such as Gaussian, uniform, and mixed noise filtering. It is also possible to extend the NLI roughness index as a general no-reference image quality metric. These are some of the interesting directions that are worth pursuing in future work.

Acknowledgment. This study was supported by the Fundamental Research Grant Scheme, Ministry of Higher Education, Malaysia, titled “Investigation of New Color Image Illumination Estimation Concept for Development of New Color Correction Techniques,” (MOHE-FRGS 203/PELECT/6071223).

REFERENCES

- [1] K. K. V. Toh, H. Ibrahim and M. N. Mahyuddin, Salt-and-pepper noise detection and reduction using fuzzy switching median filter, *IEEE Trans. Consumer Electronics*, vol.54, no.4, pp.1956-1961, 2008.
- [2] P. Civicioglu, Using uncorrupted neighborhoods of pixels for impulsive noise suppression, *IEEE Trans. Image Processing*, vol.16, no.3, pp.759-773, 2007.
- [3] Y. Dong, R. H. Chan and S. Xu, A detection statistic for random-valued impulse noise, *IEEE Trans. Image Processing*, vol.16, no.4, pp.1112-1120, 2007.

- [4] P. Chatterjee and P. Milanfar, Is denoising dead? *IEEE Trans. Image Processing*, vol.19, no.4, pp.895-911, 2010.
- [5] R. C. Gonzalez and R. E. Woods, *Digital Image Processing*, 2nd Edition, Prentice Hall, Englewood Cliffs, NJ, 2002.
- [6] J. H. Wang, W. J. Liu and L. D. Lin, Histogram-based fuzzy filter for image restoration, *IEEE Trans. Systems, Man, and Cybernetics – Part B: Cybernetics*, vol.32, no.2, pp.230-238, 2002.
- [7] S. Zhang and M. A. Karim, A new impulse detector for switching median filters, *IEEE Signal Processing Letters*, vol.9, no.11, pp.360-363, 2002.
- [8] J. Y. Chang and J. L. Chen, Classifier-augmented median filters for image restoration, *IEEE Trans. Instrumentation and Measurement*, vol.53, no.2, pp.351-356, 2004.
- [9] W. Luo, Efficient removal of impulse noise from digital images, *IEEE Trans. Consumer Electronics*, vol.52, no.2, pp.523-527, 2006.
- [10] K. S. Srinivasan and D. Ebenezer, A new fast and efficient decision-based algorithm for removal of high-density impulse noises, *IEEE Signal Processing Letters*, vol.14, no.3, pp.189-192, 2007.
- [11] S. S. Agaian, E. E. Danahy and K. A. Panetta, Logical system representation of images and removal of impulse noise, *IEEE Trans. Systems, Man, and Cybernetics – Part A: Systems and Humans*, vol.38, no.6, pp.1349-1362, 2008.
- [12] P. Y. Chen and C. Y. Lien, An efficient edge-preserving algorithm for removal of salt-and-pepper noise, *IEEE Signal Processing Letters*, vol.15, pp.833-836, 2008.
- [13] C. H. Lin, J. S. Tsai and C. T. Chiu, Switching bilateral filter with a texture/noise detector for universal noise removal, *IEEE Trans. Image Processing*, vol.19, no.9, pp.2307-2320, 2010.
- [14] X. Xu, E. L. Miller, D. Chen and M. Sarhadi, Adaptive two-pass rank order filter to remove impulse noise in highly corrupted images, *IEEE Trans. Image Processing*, vol.13, no.2, pp.238-247, 2004.
- [15] P. E. Ng and K. K. Ma, A switching median filter with boundary discriminative noise detection for extremely corrupted images, *IEEE Trans. Image Processing*, vol.15, no.6, pp.1506-1516, 2006.
- [16] H. Ibrahim, N. S. P. Kong and T. F. Ng, Simple adaptive median filter for the removal of impulse noise from highly corrupted images, *IEEE Trans. Consumer Electronics*, vol.54, no.4, pp.1920-1927, 2008.
- [17] K. K. V. Toh and N. A. Mat Isa, Noise adaptive fuzzy switching median filter for salt-and-pepper noise reduction, *IEEE Signal Processing Letters*, vol.17, no.3, pp.281-284, 2010.
- [18] Y. Dong and S. Xu, A new directional weighted median filter for removal of random-valued impulse noise, *IEEE Signal Processing Letters*, vol.14, no.3, pp.193-196, 2007.
- [19] H. Yu, L. Zhao and H. Wang, An efficient procedure for removing random-valued impulse noise in images, *IEEE Signal Processing Letters*, vol.15, pp.922-925, 2008.
- [20] U. Ghanekar, A. K. Singh and R. Pandey, A contrast enhancement-based filter for removal of random valued impulse noise, *IEEE Signal Processing Letters*, vol.17, no.1, pp.47-50, 2010.
- [21] Y. Wan, Q. Chen and Y. Yang, Robust impulse noise variance estimation based on image histogram, *IEEE Signal Processing Letters*, vol.17, no.5, pp.485-488, 2010.
- [22] S. Akkoul, R. Ledee, R. Leconge and R. Harba, A new adaptive switching median filter, *IEEE Signal Processing Letters*, vol.17, no.6, pp.587-590, 2010.
- [23] I. Aizenberg and C. Butakoff, Effective impulse detector based on rank-order criteria, *IEEE Signal Processing Letters*, vol.11, no.3, pp.363-366, 2004.
- [24] V. Crnojevic, V. Senk and Z. Trpovski, Advanced impulse detection based on pixel-wise MAD, *IEEE Signal Processing Letters*, vol.11, no.7, pp.589-592, 2004.
- [25] R. Garnett, T. Huegerich, C. Chui and W. He, A universal noise removal algorithm with an impulse detector, *IEEE Trans. Image Processing*, vol.14, no.11, pp.1747-1754, 2005.
- [26] W. Luo, An efficient detail-preserving approach for removing impulse noise in images, *IEEE Signal Processing Letters*, vol.13, no.7, pp.413-416, 2006.
- [27] R. H. Chan, C. W. Ho and M. Nikolova, Salt-and-pepper noise removal by median-type noise detectors and detail-preserving regularization, *IEEE Trans. Image Processing*, vol.14, no.10, pp.1479-1485, 2005.
- [28] J. Zhang, An efficient median filter based method for removing random-valued impulse noise, *Digital Signal Processing*, vol.20, no.4, pp.1010-1018, 2010.
- [29] M. E. Yuksel and E. Besdok, A simple neuro-fuzzy impulse detector for efficient blur reduction of impulse noise removal operator for digital images, *IEEE Trans. Fuzzy Systems*, vol.12, no.6, pp.854-865, 2004.
- [30] S. Schulte, M. Nachtegaele, V. D. Witte, D. Van der Weken and E. E. Kerre, A fuzzy impulse noise detection and reduction method, *IEEE Trans. Image Processing*, vol.14, no.5, pp.1153-1162, 2005.

- [31] M. E. Yuksel, A hybrid neuro-fuzzy filter for edge preserving restoration of images corrupted by impulse noise, *IEEE Trans. Image Processing*, vol.15, no.4, pp.928-936, 2006.
- [32] S. F. Liang, S. M. Lu, J. Y. Chang and C. T. Lin, A novel two-stage impulse noise removal technique based on neural networks and fuzzy decision, *IEEE Trans. Fuzzy Systems*, vol.16, no.4, pp.863-873, 2008.
- [33] N. I. Petrovic and V. Crnojevic, Universal impulse noise filter based on genetic programming, *IEEE Trans. Image Processing*, vol.17, no.7, pp.1109-1120, 2008.
- [34] P. Civicioglu, Removal of random-valued impulsive noise from corrupted images, *IEEE Trans. Consumer Electronics*, vol.55, no.4, pp.2097-2104, 2009.
- [35] A. Hussain, M. A. Jaffar, A. M. Mirza and A. Chaudhry, Detail preserving fuzzy filter for impulse noise removal, *International Journal of Innovative Computing, Information and Control*, vol.5, no.10(B), pp.3583-3591, 2009.
- [36] A. Hussain, M. A. Jaffar, Z. Ul-Qayyum and A. M. Mirza, Directional weighted median based fuzzy filter for random-valued impulse noise removal, *ICIC Express Letters, Part B: Applications*, vol.1, no.1, pp.9-14, 2010.
- [37] A. Hussain, M. A. Jaffar and A. M. Mirza, A hybrid image restoration approach: Fuzzy logic and directional weighted median based uniform impulse noise removal, *Knowledge and Information Systems*, vol.24, no.1, pp.77-90, 2010.
- [38] Z. F. Deng, Z. P. Yin and Y. L. Xiong, High probability impulse noise-removing algorithm based on mathematical morphology, *IEEE Signal Processing Letters*, vol.14, no.1, pp.31-34, 2007.
- [39] I. Aizenberg, C. Butakoff and D. Paliy, Impulsive noise removal using threshold Boolean filtering based on the impulse detecting functions, *IEEE Signal Processing Letters*, vol.12, no.1, pp.63-66, 2005.
- [40] G. Pok, J. C. Liu and A. S. Nair, Selective removal of impulse noise based on homogeneity level information, *IEEE Trans. Image Processing*, vol.12, no.1, pp.85-92, 2003.
- [41] F. Duan and Y. J. Zhang, A highly effective impulse noise detection algorithm for switching median filters, *IEEE Signal Processing Letters*, vol.17, no.7, pp.647-650, 2010.
- [42] P. Bouboulis, K. Slavakis and S. Theodoridis, Adaptive kernel-based image denoising employing semi-parametric regularization, *IEEE Trans. Image Processing*, vol.19, no.6, pp.1465-1479, 2010.
- [43] K. K. V. Toh and N. A. Mat Isa, Cluster-based adaptive fuzzy switching median filter for universal impulse noise reduction, *IEEE Trans. Consumer Electronics*, vol.56, no.4, pp.2560-2568, 2010.
- [44] J. G. M. Schavemaker, M. J. T. Reinders, J. J. Gerbrands and E. Backer, Image sharpening by morphological filtering, *Pattern Recognition*, vol.33, no.6, pp.997-1012, 2000.
- [45] Z. Wang, A. C. Bovik, H. R. Sheikh and E. P. Simoncelli, Image quality assessment: From error visibility to structural similarity, *IEEE Trans. Image Processing*, vol.13, no.4, pp.600-612, 2004.
- [46] F. Russo, New method for performance evaluation of grayscale image denoising filters, *IEEE Signal Processing Letters*, vol.17, no.5, pp.417-420, 2010.